https://doi.org/10.5194/bg-2022-49
Preprint. Discussion started: 21 February 2022

Eddy enhanced primary production accelerates bacterial growth in the Eastern Tropical North Atlantic

Quentin Devresse[1], Kevin W. Becker[1], Arne Bendinger[1,2], Johannes Hahn[1,3], Anja Engel[1]

[1]GEOMARHelmholtz Centre for Ocean Research Kiel, Germany,

[2] Laboratoire d'Etudes en Géophysique et Océanographie Spatiales (LEGOS), Université Toulouse, IRD, CNRS, CNES, UPS, Toulouse, France

[3] Bundesamt für Seeschifffahrt und Hydrographie, Hamburg, Germany

Correspondence: Quentin Devresse (qdevresse@geomar.de)

Abstract

Mesoscale eddies play essential roles in modulating the ocean's physical, chemical, and biological properties. In cyclonic eddies (CE) nutrient upwelling can stimulate primary production by phytoplankton. Yet, how this locally enhanced autotrophic production affects heterotrophic bacterial activities (biomass production and respiration) and consequently the metabolic balance between the synthesis and the consumption of dissolved organic matter (DOM) remains largely unknown. To address this gap, we investigated the horizontal and vertical variability of phytoplankton and heterotrophic bacterial activity along ~900 km zonal corridor between the coast of Mauretania and the Cape Verde Islands in the eastern tropical North Atlantic (ETNA). We additionally collected samples from a CE along this transect at high spatial resolution. Our results show cascading effects of physical disturbances induced by a CE on phyto- and bacterioplankton biomass and metabolic activities. Specifically, the injection of nutrients into the sunlit surface resulted in enhanced autotrophic plankton abundance and activity as indicated by Chlorophyll *a* (Chl-*a*) concentration, DOM exudation, and primary productivity (PP). However, the detailed eddy survey revealed an uneven distribution of these parameters with, for example, the highest Chl-*a* concentrations and PP rates near and just beyond the CE's periphery. The heterotrophic bacterial activity was similarly variable. Optode-based bacterial respiration (BR) and biomass production (BP) largely followed the trends of PP and Chl-*a*. Thus, a submesoscale spatial mosaic of heterotrophic bacterial abundance and activities occurred within the CE studied here that was closely related to variability in autotrophic production. This was supported by a significant positive correlation

https://doi.org/10.5194/bg-2022-49
Preprint. Discussion started: 21 February 2022

between concentrations of semi-labile organic carbon (SL-DOC; the sum of dissolved hydrolyzable amino acids and combined carbohydrates) and BR measurements. Bacterial growth efficiency (BP/(BR+BP)) was variable (1.4-10.5%) within the CE and carbon exudation was not always sufficient to compensate the bacterial carbon demand (BR+BP; 28.3-114.5%). We have additionally estimated the metabolic state in our samples, which showed that the CE carried a strong autotrophic signal (PP/(BR+BP)>1). Overall, our results show that submesoscale (0-10 km) processes lead to highly variable metabolic activities of both phototrophic and heterotrophic microbes, which has implications for biogeochemical models estimating oceanic carbon fluxes. Additionally, we revealed that the CE not only traps and transports coastal nutrients and carbon to the open ocean but also stimulates phytoplankton growth generating freshly produced organic matter during westward propagation. This organic matter may fuel heterotrophic processes in the open ocean and may help to explain the often-observed net heterotrophic metabolic state of these environments.

1. Introduction

Mesoscale eddies (10-100 km) are ubiquitous in the ocean affecting upper ocean biogeochemistry and ecology, e.g. upwelling nutrients influencing primary production and carbon export (Cheney and Richardson, 1976; Arístegui et al., 1997). The sense of rotation and their vertical structure classifies cyclonic (CEs), anticyclonic (ACEs; e.g. Chelton et al., 2011) or anticyclonic mode water eddies (ACMEs; D'Asaro 1988). In Eastern Boundary Upwelling Systems (EBUS), eddies may form by flow separation of along slope boundary currents at topographic headlands (D'Asaro 1988, Molemaker et al., 2015, Thomsen et al., 2016). Eddies have lifespans from days to months and can travel several hundred to thousands of kilometers across ocean basins (Chelton et al., 2011). They are complex dynamical regimes for organic matter and nutrient transport (Gruber et al., 2011). In the North Atlantic Ocean, eddies generated in the highly productive Canary Upwelling System (CanUS) may laterally propagate to the oligotrophic Subtropical North Atlantic Gyre (SNAG), transporting thereby nutrients and carbon (McGillicuddy et al., 2003; Karstensen et al., 2015; Schütte et al., 2016). A variety of studies demonstrated the impact of eddies on primary production (PP) on a global scale. Yet, the magnitude of the eddy-induced flux and its utilization depend on the model, the area investigated, and the degree of resolution and is still controversial (See review by McGillicuddy, 2016 and references therein). For example, Couespel et al., (2021) performed

https://doi.org/10.5194/bg-2022-49
Preprint. Discussion started: 21 February 2022

global warming simulations using a representation of mid-latitude double-gyre circulation and showed that at the finest model resolution (1/27°), eddies can mitigate the decline of primary production (−12 % at 1/27° vs. −26 % at 1°). Modeling studies have long urged consideration of the effects of eddies on PP at submesoscale levels (0.1-10 km) to provide realistic estimates of the oceanic carbon cycle (Levy et al., 2001). Thus, understanding the impact of mesoscale eddies on plankton productivity will help to better predict future carbon cycling in EBUS under global change scenarios.

Eddies modulate the mixed layer depth by upwelling (CEs), downwelling (ACEs), or frontogenesis from eddy-eddy interaction, thereby creating spatial variability of nutrient concentration within/around eddies on length scales of 0.1-10 km (see reviews by Mahadevan, 2016 and McGillicuddy, 2016). In addition, the nonlinear response of phytoplankton growth to nutrient availability and advection of phytoplankton by currents makes plankton distribution and community composition highly variable within and around eddies (Lochte and Pfannkuche 1987). As a consequence, the spatial distribution of PP across eddies can be highly variable (e.g. Falkowski et al., 1991; Ewart et al., 2008; Singh et al., 2015). Still, insight into the distribution of phytoplankton and their activities within mesoscale eddies is limited due to a lack of sufficient fine-scale vertical and horizontal resolution studies to adequately describe these distributions.

Bacterial activity is directly coupled to PP: autotrophic cells release dissolved organic matter (DOM), the main substrate for heterotrophic bacteria and archaea (Thornton 2014). DOM release has been interpreted as a cellular overflow mechanism that expels the carbon produced in excess (Wood and Van Valen, 1990; Schartau et al., 2007). Therefore, released DOM compounds are often depleted in nutrients limiting autotrophic cell growth (Engel et al., 2002). Patchiness of phytoplankton primary productivity and nutrient limitation within eddies may thus lead to spatial heterogeneity of extracellular release rates (e.g. Lasternas et al., 2013, Rao et al., 2021) with distinct quality (e.g. Wear et al., 2020). DOM quality impacts biomass production (BP), bacterial respiration (BR), and, thus the bacterial growth efficiency (BGE; Neijssel and de Mattos, 1994; Russell and Cook, 1995). BGE is the ratio between BP and the bacterial carbon demand (BCD), which is the sum of assimilated carbon that is respired and carbon that is incorporated into biomass (BP + BR). Lønborg et al., (2011) established that BGE decreases with increasing C/N ratio of the bioavailable DOM produced by phytoplankton. BGE is a critical parameter for estimating the amount of consumed organic carbon that is used to build biomass by heterotrophic bacteria (Anderson and Ducklow 2001). So far, BGE within

https://doi.org/10.5194/bg-2022-49
Preprint. Discussion started: 21 February 2022

eddies has been reported for ACEs from the Mediterranean Sea (Christaki et al., 2011), but not for CEs and Mode Water Eddies. In general, several studies showed a patchy distribution of bacterial abundance, BP (Ewart et al., 2008; Baltar et al., 2010), BR, community respiration (CR) (Mouriño-Carballido and McGillicuddy 2006; Mouriño-Carballido, 2009), and of the metabolic balance between production and consumption of organic matter (Maixandeau et al., 2005; Ewart et al., 2008; Mouriño-Carballido and McGillicuddy 2006; Mouriño-Carballido, 2009) within eddies.

Yet, how eddies affect microbial plankton dynamics and carbon flow is largely unknown. So far, phyto- and bacterioplankton distribution and activities were either studied separately or at relatively low spatial resolution. Data on eddy-induced changes in primary production, extracellular release and semi-labile DOM concentration, and the responses of heterotrophic microbial metabolic activities are scarce. Understanding how eddies modulate microbial activities will enhance our knowledge about the fate of autotrophically fixed organic carbon and the overall CO_2 source/sink function in the ocean, and in particular EBUS.

Here, we studied the impact of a CE on microbial carbon cycling along a zonal corridor of the westward propagating eddies between the Cape Verde Islands and the Mauretania Upwelling System 13-20 °N), a sub-region of the CanUS (13-33 °N, Arístegui et al., 2009). About 146 ± 44 eddies with a lifetime of more than 7 days are generated per year in this region (Schütte et al., 2016). Along this corridor, we determined phytoplankton (<20µm) cell abundance, primary production, and extracellular release. We linked those parameters of autotrophic activity to semi-labile DOM concentration and heterotrophic bacterial activity. Our study gives new insights into 1) microbial carbon cycling and 2) factors controlling microbial metabolic activities within and around CE formed in EBUS.

2. Materials and Methods

2.1 Study area and eddy characterization

Sampling was conducted in the ETNA between the Cape Verde archipelago and the Mauritanian coast during cruise M156 (July 3rd to August 1st, 2019. Figure **1A**) on the R/V *Meteor*. Samples were collected during the relaxation period (from May to July) that follows the upwelling season (January to March; Lathuilière et al., 2008). A CE was sampled at high

https://doi.org/10.5194/bg-2022-49
Preprint. Discussion started: 21 February 2022

spatial resolution along two zonal (from 19.1 °W to 18.2 °W at 18.3 °N and from 18.5 °W to 17.1 °W at 18.6 °N) and one meridional transects (from 19.4 °N to 18 °N at 18.4 °W to 18.1 °W). The zonal section was slightly meridionally shifted east/west of the eddy core position. The reason for that was the deformed eddy shape, which resulted in a consecutive optimized identification of the eddy core position during the eddy survey. In addition, we sampled water along the 18 °N transect, a typical coast to open ocean trajectory of eddies in the region (Schütte et al., 2016). Salinity, temperature, depth, and O_2 concentration were determined at each station using a Seabird 911 plus CTD system equipped with two independently working sets of temperature-conductivity-oxygen sensors. The oxygen sensor was calibrated against discrete water samples using the Winkler method (Strickland and Parsons, 1968; Wilhelm, 1888). Seawater samples were collected from the top 200 m using 10L Niskin bottles attached to the CTD Rosette. A total of 25 stations were sampled; 14 of them inside or in the vicinity of the CE. Sampling was conducted in the epipelagic layer (0-200 m), including water from the surface, within the mixed layer, at the Chl-*a* maximum, and within the shallow oxygen minimum zone (OMZ; <50 µmol kg^{-1} between 0-200 m depth) when present.

Sea surface height (SSH) and Acoustic Doppler Current Profiler (ADCP) velocity data (SI Fig. **1**), characterized the eddy as a CE. Based on the Angular Momentum Eddy Detection and Tracking Algorithm (AMEDA; Le Vu et al., 2018), the eddy was estimated to be 1.5 months old. The center of the eddy and the core radius were determined using ADCP reconstruction assuming an axis-symmetric vortex. (SI Fig. **1**). On 22/07/2019, the eddy center was located at 18.69 °N, 18.05 °W, with a core radius of 40.5 ± 5.7 km. The mean azimuthal velocity in the CE was 19.9 ± 0.7 cm s^{-1} and the absolute dynamic topography associated with the CE core was ~23 cm on 23/07/19. Fine-scale analysis of the eddy physics will be given by Fischer et al. (2022, in prep). However, as the eddy shape was deformed, ADCP reconstruction did not constrain well the physical border of the eddy (SI Fig. **1**). Therefore, we combined sea surface temperature (23.44 ± 0.47 °C) salinity (39.95 ± 0.04) and Chl-*a* (1.35 ± 0.73 µg L^{-1}) data to approximate the area influenced by the eddy (Fig. **1b**,**c**,**d**). We classified stations into 'core' and 'periphery' of the eddy. Stations that were outside and westward of the eddy influence were referred to as 'open ocean' and those close to the coast as 'coastal'. At the St. E3, outside of the CE periphery, we observed a front with surface temperature and salinity (not compensating in density) being clearly different from among the adjacent stations (Fig. **1b**), potentially which might be related to enhanced, an up- and downwelling might have occurred there on either side of the front, respectively. Hence, we referred to that station as 'Frontal Zone'. The classification of stations is thoroughly discussed in the supplementary information (SI), and the sampling time, location, and distance from the eddy center are given in Table S**1**.

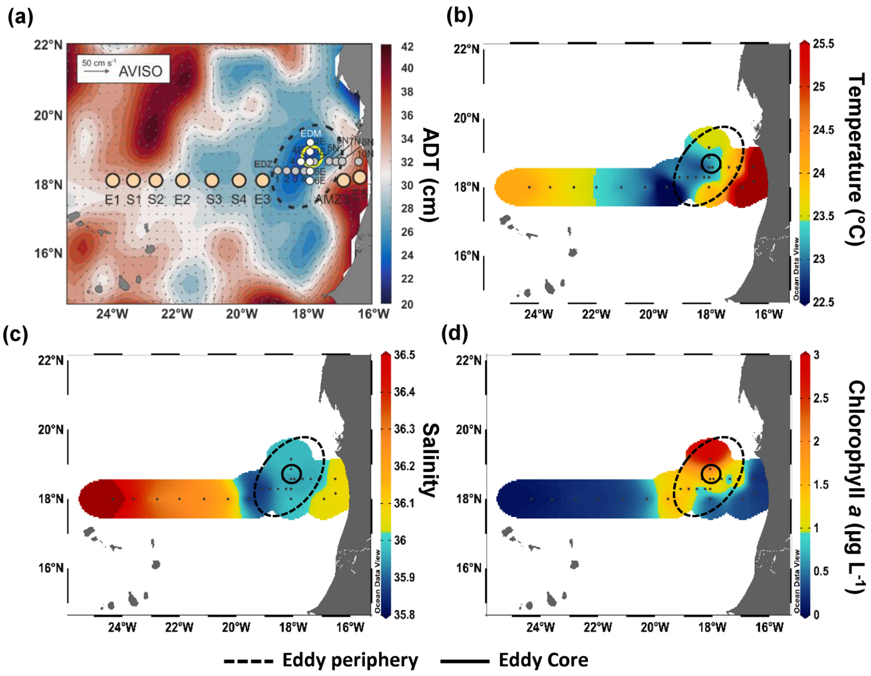

Figure 1: M156 cruise track (**a**) Temperature at 5m depth (**b**) Salinity at 5m depth (**c**) chlorophyll a at 5m depth (**d**). The color background in (**a**) shows the variations in Absolute Dynamic Topography (ADT). The direction and speed of surface water geostrophic currents are shown as arrows.

2.2 Chemical analyses

Nutrient concentrations were determined at selected stations (SI Table **1**). Nutrients were measured onboard from duplicate samples (11 mL) of unfiltered seawater samples. Ammonium (NH_4^+) was analyzed after Solórzano (1969) and phosphate (PO_4), nitrate (NO_3), nitrite (NO_2), and silicate ($Si(OH)_4$) were measured photometrically with continuous-flow analysis on an auto-analyzer (QuAAtro; Seal Analytical) after Grasshoff et al., (1999). Detection limits for NH_4^+, PO_4, NO_3, NO_2, and $Si(OH)_4$ were 0.1, 0.02, 0.1, 0.02, and 0.2 µmol L^{-1}, respectively Total dissolved inorganic nitrogen (DIN) was determined as the sum of NH_4^+, NO_3, and NO_2.

To estimate the fraction of semi-labile dissolved organic carbon (DOC), we determined high-molecular-weight (HMW> 1 kDa) dissolved combined carbohydrates (dCCHO) and dissolved amino acids (dAA) as the main biochemical components of DOM.

Duplicate samples (20 mL) for dCCHO were filtered through 0.45 µm Acrodisk filters, collected in combusted glass vials (8 h, 450 °C) and frozen (−20 °C) until analysis after Engel & Händel (2011) with a detection limit of 1 µg L^{-1}. The analysis detected 11 monomers: arabinose, fucose, galactose, galactosamine, galacturonic acid, glucosamine, glucose, glucuronic acid, rhamnose, co-elute mannose, and xylose.

Duplicate samples (4 mL) for dHAA were filtered through 0.45µm Acrodisk filters, collected in combusted glass vials (8 h, 450 °C), and frozen (−20 °C) until analysis. dAA were measured with ortho- phthaldialdehyde derivatization by high-performance liquid chromatography (HPLC; Agilent Technologies, USA) equipped with a C_{18} column (Phenomenex, USA) (Lindroth and Mopper, 1979; Dittmar et al., 2009). The analysis classified 13 monomers with a precision < 5 % and a detection limit of 2 nmol L^{-1}: alanine, arginine, aspartic acid, isoleucine, glutamic acid, glycine, leucine, phenylalanine, serine, threonine, tyrosine, valine; and γ-aminobutyric acid (GABA).

The calculations for the carbon content of dCCHO and dHAA were based on carbon atoms contained in the identified monomers. The sum of dCCHO and dHAA carbon content is referred to as semi-labile DOC (SL-DOC).

For Chl-*a,* 1L samples were collected on 25 mm GF/F (Whatman, GE Healthcare Life Sciences, UK) and subsequently frozen (−20 °C) until extraction using 90 % acetone for photometric analyses (Turner Designs, USA), slightly modified after Evans et al., (1987).

Bacteria were quantified using a flow cytometer (FACSCalibur, Becton Dickinson, Oxford, UK). Seawater samples (1.7 mL) were fixed with 85 µL glutaraldehyde (1% final concentration) and stored at -80 °C until enumeration. Samples were stained with SYBR Green I (molecular probes) and were enumerated with a laser emitting at 488 nm and detected by their signature in a plot of side scatter (SSC) vs green fluorescence (FL1). Heterotrophic bacteria were distinguished from photosynthetic bacteria (*Prochlorococcus* and *Synechococcus*) by their signature in a plot of red fluorescence (FL2) vs green fluorescence (FL1). Yellow-green latex beads (1 µm, Polysciences) were used as an internal standard. (Stolle et al., 2009). Cell counts were determined with the CellQuest software (Becton Dickinson). For autotrophic pico and nanoplankton <20 µm, 2 mL samples were fixed with formaldehyde (1 % final concentration) and stored frozen (−80 °C) until analysis. Red and orange autofluorescence was used to identify Chl-*a* and phycoerythrin cells. Cell counts were determined with CellQuest software (Becton Dickinson); picoplankton and nanoplankton populations containing Chl-*a* and/or phycoerythrin (i.e., *Synechococcus*) were identified and enumerated. We converted the cell abundance of the different autotrophic plankton populations into biomass assuming 43 fg C cell^{-1} for *Prochlorococcus*, 120 fg C cell^{-1} for *Synechococcus*, 500 fg C cell^{-1} for eukaryotic picoplankton and, 3.100 fg C cell^{-1} for eukaryotic nanoplankton after Hernández-Hernández et al., (2020). We report the autotrophic plankton biomass as the sum of eukaryotic pico- and nanoplankton and cyanobacteria (*Prochlorococcus* and *Synechococcus*) biomass. The abundance of eukaryotic pico- and nanoplankton and cyanobacteria (*Prochlorococcus* and *Synechococcus*) can be found in the SI (Table S**2**).

2.3 Microbial activities

More information on procedures and calculations of microbial activities are given in the SI.

Bacterial biomass production rates (BP) were measured through the incorporation of labeled leucine (^{3}H) (specific activity 100 Ci mmol^{-1}, Biotrend) using the microcentrifuge method (Kirchman et al., 1985; Smith and Azam, 1992). Duplicate samples and one killed control (1.5 mL each) were labeled using ^{3}H-leucine at a final concentration of 20 nmol L^{-1} and incubated with headspace for 6 h in the dark at 14 °C. Controls were poisoned with trichloroacetic acid. All Samples were measured on board with a liquid scintillation analyzer (Packard Tri-Carb, model 1900 A). ^{3}H-leucine uptake was converted to carbon units applying a conversion factor of 1.55 kg C mol^{-1} leucine (Simon and Azam, 1989).

BP rates at 22 °C were estimated following López-Urrutia and Morán (2007):

$$\mathrm{BP}_{22°\mathrm{C}} = BP_{14°C} \times 0.996 \qquad \text{(Eq. 1)}$$

Community respiration rates (CR) were estimated from changes of dissolved oxygen in 24-36 hours incubations at 14°C using optode spot mini sensors (PreSens PSt3; Precision Sensing GmbH, Regensburg, Germany). The detection limit (DL) for CR was 0.55 µmol O_2 L^{-1} d^{-1}.

CR at 22°C was estimated using extrapolation from Regaudie-De-Gioux and Duarte (2012):

$$\mathrm{CR}_{22°\mathrm{C}} = CR_{14°C} \times 2.011 - 0.013 \quad \text{(Eq. 2)}$$

$\mathrm{CR}_{22°\mathrm{C}}$ was converted into bacterial respiration ($\mathrm{BR}_{22°\mathrm{C}}$) after Aranguren-Gassis et al. (2012):

$$\mathrm{BR}_{22°\mathrm{C}} = 0.30 \times \mathrm{CR}_{22°\mathrm{C}}{}^{1.22} - 0.013 \qquad \text{(Eq. 3)}$$

A respiratory quotient of 1 was used to convert oxygen consumption into carbon respiration (del Giorgio and Cole 1998).

We furthermore estimated the bacterial carbon demand (BCD):

$$BCD = BP + BR \qquad \text{(Eq. 4)}$$

and the bacterial growth efficiency (BGE):

$$BGE = \frac{BP}{BCD} \qquad \text{(Eq. 5)}$$

Primary production (PP) was determined from ^{14}C incorporation according to Steemann Nielsen (1952) and Gargas (1975). Polycarbonate bottles (Nunc EasYFlask, 75 cm^2) were filled with 260 mL prefiltered (mesh size of 200 µm) sample and spiked with 50 µL of a ~11 µCi $NaH^{14}CO_3^-$ solution (Perkin Elmer, Norway). 200 µL were removed immediately after spiking and transferred to a 5 mL scintillation vial for determination of added activity. Then, 50 µL of 2N NaOH and 4 mL scintillation cocktail (Ultima Gold AB) were added. Duplicate samples were incubated in 12 h light and 12 h dark at 22 °C. Three light levels were applied: 1200-1400; 350 and 5 µE, with high values representing surface irradiance at the time of sampling. The incubation length was chosen for two reasons. First, we expected low productivity of the open ocean phytoplankton community due to low biomass and low nutrient concentrations at the start of the incubation. Under these conditions, short-term incubations of only a few hours may underestimate PP, because carbon assimilation by algal cells may be too low to discriminate against ^{14}C adsorption as determined in blank dark incubation (Engel et al., 2013). Moreover, the release of freshly assimilated carbon into the DOM pool has a time scale of several hours because of the equilibration of the tracer and because metabolic processes of organic carbon exudation follow those of carbon fixation inside the cell (Engel et al., 2013). Incubations were stopped by filtration of a 70 mL sub-sample onto 0.4 µm polycarbonate filters (Nuclepore). Particulate primary production (PP_{POC}) was determined from material collected on the filter, while the filtrate was used to determine dissolved primary production (PP_{DOC}). All filters were rinsed with 10 mL sterile filtered (<0.2 µm) seawater, and then acidified with 250 µL 2N HCl to remove inorganic carbon (Descy et al., 2002). Filters were transferred into 5 mL scintillation vials, and 4 mL scintillation cocktail (Ultima Gold AB) was added. To determine PP_{POC} and PP_{DOC}, 4 mL of filtrate and incubated sample were transferred to 20 mL scintillation vials, acidified (100 µL 1N HCl), and left open in the fume hood to remove inorganic carbon. Then, 100 µL of 2N NaOH and 15 mL scintillation cocktail were added. All samples were counted the following day in a liquid scintillation analyzer (Packard Tri-Carb, model 1900 A).

Primary production (PP) of organic carbon was calculated according to Gargas (1975):

$$\mathrm{PP}\ (\mu\mathrm{molC\ L^{-1}\ d^{-1}}) = \frac{a2 \times DI^{12}C \times 1.05 \times k_1 \times k_2}{a1} \qquad \text{(Eq.6)}$$

Where $a1$ and $a2$ are the activities (DPM) (disintegrations per minute) of the added solution and the sample corrected for dark sample, respectively, and $\mathrm{DI^{12}C}$ is the concentration (µmol $\mathrm{L^{-1}}$) of dissolved inorganic carbon (DIC) in the sample. Dissolved inorganic carbon concentration was calculated from total alkalinity using r package seacarb (Gattuso et al., 2020). Total alkalinity of the seawater was acquired through the open-cell titration method (Dickson et al., 2007). The value 1.05 is a correction factor for the discrimination between ^{12}C and ^{14}C, as the uptake of the ^{14}C isotope is 5% slower than the uptake of ^{12}C, k_1 is a correction factor for subsampling (bottle volume/filtered volume) and k_2 is the incubation time ($\mathrm{d^{-1}}$). Total primary production ($\mathrm{PP_{TOT}}$; µmol C $\mathrm{L^{-1}\ d^{-1}}$) was derived from the sum of $\mathrm{PP_{POC}}$ and $\mathrm{PP_{DOC}}$ according to:

$$\mathrm{PP}_{TOT} = \mathrm{PP_{POC}} + \mathrm{PP_{DOC}} \qquad \text{(Eq.7)}$$

The percentage of extracellular release (PER; %) was calculated as:

$$\mathrm{PER} = \left(\frac{\mathrm{PP_{DOC}}}{\mathrm{PP}_{TOT}}\right) \times 100 \qquad \text{(Eq.8)}$$

2.4 Data analysis

Statistical analyses and calculations were conducted using the software R (v4.0.3) in Rstudio (v1.1.414; Ihaka and Gentleman 1996). Analysis of variances (ANOVA) and Tukey test, were performed on the different parameters by grouping the station by their position (SI Table **1**). Seawater density was calculated using r package oce v1.3.0 (Kelley, 2018) and mixed layer maximum depth was determined as the depth at which a change from the surface density of 0.125 has occurred (Levitus, 1982). Section plots were realized using Ocean Data View (Schlitzer, 2020). Other packages used in this study include corrplot v0.84 (Dray, 2008) and ggplot2 v3.3.3 (Wickham, 2016). Depth integrated values were calculated using the midpoint rule.

https://doi.org/10.5194/bg-2022-49
Preprint. Discussion started: 21 February 2022

3. Results

3.1 Hydrographic conditions

Along the zonal transect, open ocean waters (from 20 to 24.5 °W) had a temperature range of 17.0-24.3 °C and salinity of 36.19-36.79 in the upper 150m depth (Fig. **2a** & **b**). The average mixed layer depth was 30 ± 2 m (SI Table **1**). Oxygen concentration (Fig. **2c**) decreased with depth while nutrient concentrations increased (Fig. **2d-e**). Nutrients were depleted (<0.5, <0.2, and <0.5 µmol L^{-1} for DIN, PO_4, $Si(OH)_4$, respectively) in the mixed layer.

At the coastal stations (16.51 to 16.92 °W), the temperature had a range of 14.6-26.1 °C and salinity of 35.53-36.08 in the upper 150 m depth (Fig. **2a** & **b**). Here, the mixed layer was significantly shallower than in the open ocean (Tukey, $p<0.01$), with an average depth of 17 ± 4 m (SI Table **1**). Oxygen was decreasing with depth and a shallow oxygen minimum (OMZ; <50 µmol kg^{-1}) was detected (Fig. **2c**) from 80 m to 200 m depth. Nutrients (Fig. **2d-e**) were depleted at the surface (5 m depth) while the deeper coastal waters (~ 80 to 200 m depth) were colder and richer in nutrients than in the open ocean with on average 3.4 fold more nutrients (DIN, PO4, $Si(OH)_4$) when integrated over 100 m depth.

In the CE ('periphery' and 'core'), waters had a temperature range of 13.5-24.2 °C and salinity of 35.48-36.36 in the upper 150 m depth (Fig. **2a** & **b**). A tightening of isopycnals with a strong doming of the isotherms, isohalines, and nutriclines was observed (Fig. **2a-b**, **d-f**). A shallow OMZ was detected from ~30m to ~100 m depth with the lowest oxygen concentration (<10 µmol kg^{-1}) between 30-40 m depth. The mixed layer was significantly shallower (Tukey, $p<0.05$) at the CE periphery than in the open ocean, with an average of 15 ± 6 m depth. However, the CE core was not significantly different (21 ± 3 m; Tukey, $p>0.05$). Nutrients **(**Fig. **2d-f**) were depleted (<0.5, <0.2 and <0.5 µmol L^{-1} for DIN, PO_4, $Si(OH)_4$ respectively) at the surface (~5 m) only in the Eastern (17.11 °W, 18 °N) and Western (18.83-19.11 °W, 18.58 °N) part of the CE periphery.

The Frontal Zone station E3 (19.55 °W) was distinct from the adjacent stations with respect to surface temperature (1 °C colder, Fig **2a**). A doming of the nutriclines was observed **(**Fig.**2d-f**) and nutrient concentrations integrated over 100 m depth at St. E3 were ~3 fold higher than Open ocean St. S4 (20.3 °W) and ~1.2 fold higher than CE periphery St. EDZ-1 (19.11 °W).

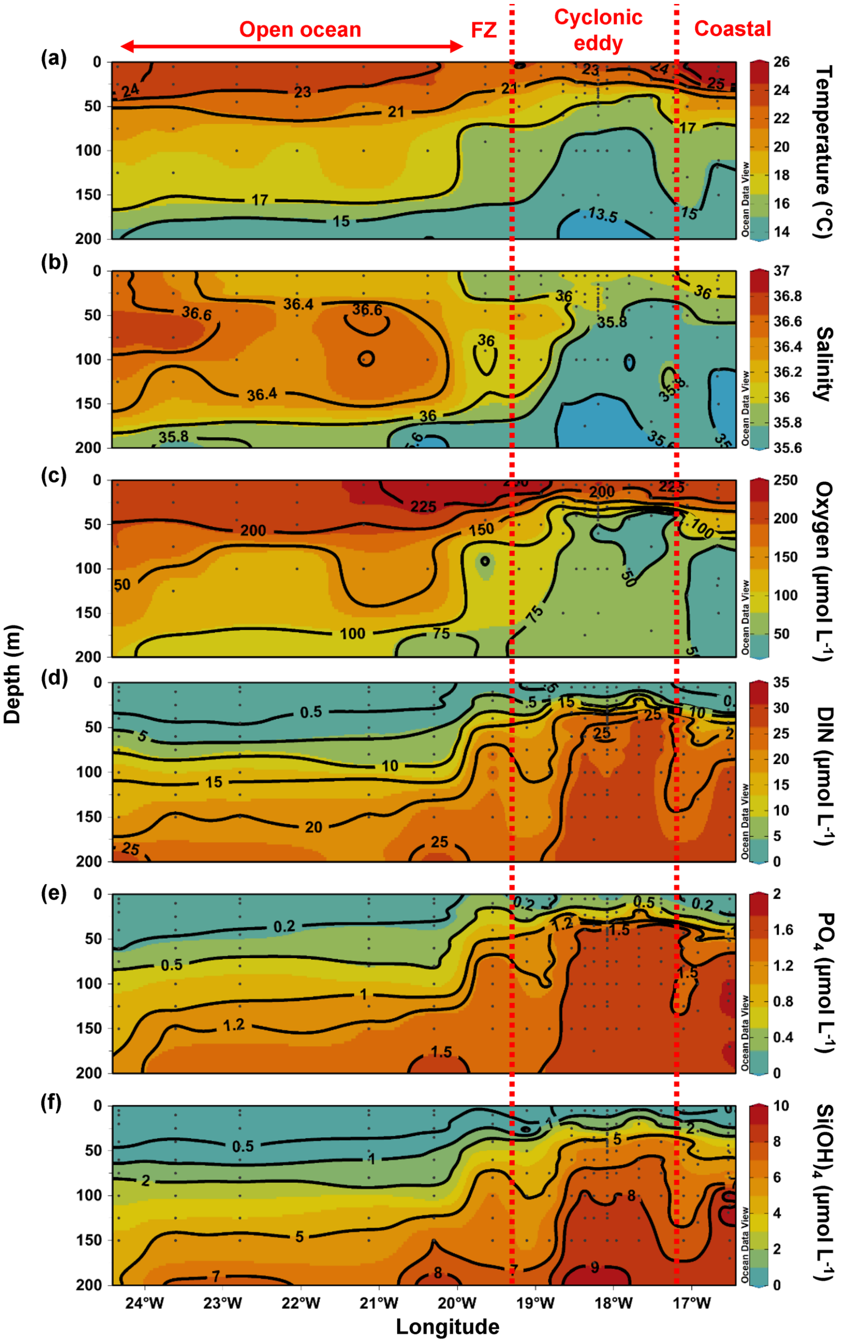

Figure 2: Epipelagic distribution (0-200m) of Temperature (**a**), Salinity (**b**), Oxygen (**c**), Total inorganic nitrogen (DIN, **d**), PO_4 (**e**), $Si(OH)_4$ (**f**). Red dashed line show the cyclonic eddy periphery and FZ refer as Frontal Zone.

https://doi.org/10.5194/bg-2022-49
Preprint. Discussion started: 21 February 2022

3.2 Chlorophyll-*a* and primary production

In order to compare stations along the zonal transect and within the eddy, data were integrated over the water column (0-100 m depth). Along the zonal transect, depth-integrated Chl-*a* concentration ranged between 11.7 and 58.7 mg m^{-2} and decreased from the coastal to the open ocean stations (Table **1**; SI Fig. **S4**). Depth-distribution (Fig. **3a**) presented a Chl-*a* maximum in the open ocean around ~75 m from 23.61 to 24.33 °W and around ~50 m from 22.78 to 20.3 °W, up to 0.70 µg L^{-1}. At the coastal stations, the Chl-*a* maximum was found between 30-40 m depth with values up to 0.96 µg L^{-1}. Integrated autotrophic plankton biomass (Table **1**) ranged between 1.6 and 7.8 and between 3.6 and 6.1 g C m^{-2} in the open ocean and at the coastal stations, respectively. In the open ocean waters, autotrophic plankton biomass (Fig. **3b**) presented a gradient of distribution with a maximum around ~75 m from 23.61 to 24.33 °W, around ~50 m from 22 to 22.78 °W and between 5-25 m from 21.13 to 20.3 °W, with values up to 166 µg C L^{-1}. In the coastal stations, autotrophic plankton biomass maximum was found between 30-40 m depth with values up to 117 µg C L^{-1}. Both Chl-*a* concentration and autotrophic plankton biomass did not vary significantly between the open ocean and the coastal stations (Tukey, $p>0.05$). Integrated total and dissolved primary production (PP_{TOT}; PP_{DOC}; Table **1**) remained fairly constant with ranges of 101-137 and 42.8-78 mmol C m^{-2} d^{-1}, respectively, from the coastal to the open ocean stations, except for the station furthest offshore (24.33 °W), where rates decreased sharply to 25.8 mmol C m^{-2} d^{-1} for PP_{TOT} and to 12.3 mmol C m^{-2} d^{-1} for PP_{DOC}. The integrated percentage of extracellular release (PER; Table 1) in both regions ranged between 42.3-67.5%. Both PP_{TOT} and PER did not vary significantly between the open ocean and the coastal stations (Tukey, $p>0.05$). PP_{TOT} was decreasing with depth (Fig. **3c**) while PER was increasing (Fig. **3d**). In general, PP_{TOT} and PP_{DOC} were positively correlated to the Chl-*a* concentration ($R^2=0.48$ and 0.42 respectively; $p<0.001$; Fig. **6c** & **d**).

In the CE (core and periphery) and at the Frontal Zone integrated Chl-*a* concentration ranged from 17.2 to 225 mg m^{-2} (Table **1**). The Chl-*a* distribution (SI Fig. **S4**) showed a clear spatial separation with the highest values (98.7-225 mg m^{-2}) in the western (18.83-19.11 °W, 18.29 °N) and northern (148 mg m^{-2}; 18.08 °W, 19.15 °N) part of the CE and lowest values (26.8-37.5 mg m^{-2}) in the eastern in the Southern (18.08 °W, 18 °N) and Eastern part (17.39 - 17.68 °W, 18.58 °N). Depth distribution of Chl-*a* concentration also differed across the eddy, with values >0.5 µg L^{-1} reaching down to 45 m depth at the Frontal Zone and the western part of the CE (19.11-19.55 °W) and down to 30 m depth in the eastern side of the CE (17.1-17.4 °W). Within the upper 30 m, Chl-*a* concentration within the CE was significantly higher than at the open ocean and the coastal stations (ANOVA, $p<0.05$). Integrated autotrophic plankton biomass ranged between 0.3 and 4.7 g C m^{-2} in the CE (Table **1**). Depth distribution of autotrophic plankton biomass (Fig. **3b**) showed low biomass in the upper 40 m (<25 µg C L^{-1}) from 18.83 to 19.11 °W. In contrast, higher biomass (>25 µg C L^{-1}) occurred in the more eastern stations of the CE (17.11 to 18.54 °W) and westwards from the Frontal Zone (19.55 °W). In the eddy, autotrophic plankton biomass reached higher concentrations mostly within the upper 40 m, with values up to 191 µg C L^{-1}. It should be noted that autotrophic biomass refers only to pico- and nanophytoplankton and not to larger cells such as typical for diatoms or dinoflagellates. Depth-integrated PP$_{\mathrm{TOT}}$ and PP$_{\mathrm{DOC}}$ rates were significantly higher in the CE and at the Frontal Zone than at the open ocean and the coastal stations (Tukey, $p<0.05$) with values ranging from 245 to 687 mmol C m^{-2} d^{-1} and from 95.9 to 238 mmol C m^{-2} d^{-1}, respectively (Table **1**). PP$_{\mathrm{TOT}}$ rates (Fig. **2c**; Table **2**) were fairly constant across the CE's surface (5 m depth), ranging between 11.7 to 13.3 µmol C L^{-1} d^{-1}, but varied strongly between 15-40 m depth with values from 0.2 to 14.5 µmol C L^{-1} d^{-1}. The highest PP$_{\mathrm{TOT}}$ rates were found in the Frontal Zone with up to 25.0 µmol C L^{-1} d^{-1} at the surface. The range of PP$_{\mathrm{DOC}}$ rates (Table **2**) was larger in the CE (0.2-4.9 µmol C L^{-1} d^{-1}) and the Frontal Zone (0.7-7.8 µmol C L^{-1} d^{-1}) than in the open ocean and at the coastal stations. Integrated PER had a range of 29.4-43.3 % (Table **1**). A slightly lower PER was observed within the upper 40 m (Fig. **2d**) for the CE and Frontal Zone compared to open ocean and coastal stations.

Table 1: Chlorophyll a (Chl *a*) and abundance, biomass and activity of phyto- and bacterial plankton, integrated over the upper 100m depth. '-' indicate that the parameter was not measured. PP$_{\mathrm{DOC}}$ and PP$_{\mathrm{TOT}}$ rates in St EDM-4E were measured on the 22/07/2019 from 5, 33 and 50m depth and CR and BR rates were measured in St. E5 on the 29/07/2019 from 5, 35 and 50m depth.

Location	Station	Chl *a* (mg m^{-2})	AutPl (g C m^{-2})	PP$_{\mathrm{DOC}}$ (mmol C m^{-2} d^{-1})	PP$_{\mathrm{TOT}}$ (mmol C m^{-2} d^{-1})	PER (%)	HB (10^{15} cell m^{-2})	CR (mmol C m^{-2} d^{-1})	BR (mmol C m^{-2} d^{-1})	BP (mmol C m^{-2} d^{-1})
Coastal	E5	54.5	6.1	75.2	137	54.9	14.7	99.6	32	2.9
	EDZ-10N	36.8	3.6	-	-	-	13.8	-	-	4.1
	AZM-3	58.7	5.3	-	-	-	12.9	-	-	5.7
Eddy Periphery	EDZ-8N	61.5	4.7	-	-	-	10.7	-	-	8.2
	EDZ-7N	26.8	1.6	-	-	-	9.4	-	-	5.7
	EDZ-6N	27.9	1.2	-	-	-	9.1	-	-	4.0
Eddy Core	EDZ-5N	39.2	4.1	-	-	-	14.5	154	59.1	4.7

Table 1 cont.: Chlorophyll a (Chl *a*) and abundance, biomass and activity of phyto- and bacterial plankton, integrated over the upper 100m depth. '-' indicate that the parameter was not measured. PP_{DOC} and PP_{TOT} rates in St EDM-4E were measured on the 22/07/2019 from 5, 33 and 50m depth and CR and BR rates were measured in St. E5 on the 29/07/2019 from 5, 35 and 50m depth.

Location	Station	Chl *a* (mg m^{-2})	AutPl (g C m^{-2})	PP_{DOC} (mmol C m^{-2} d^{-1})	PP_{TOT} (mmol C m^{-2} d^{-1})	PER (%)	HB (10^{15} cell m^{-2})	CR (mmol C m^{-2} d^{-1})	BR (mmol C m^{-2} d^{-1})	BP (mmol C m^{-2} d^{-1})
Eddy Core	EDM-4E	46.0	3.3	95.9	245	39.2	15.2	135	60.8	4.5
	EDM-3E	77.5	3.2	-	-	-	15.3	-	-	8.6
Eddy Periphery	EDM-4	63.8	3.3	141	380	37.2	19.4	275	127	6.4
	S5	35.7	3.6	117	288	40.8	23.7	-	-	6.8
	EDM-5E	35.2	1.6	-	-	-	11.8	-	-	4.7
	EDM-2E	148	1.7	-	-	-	20.8	-	-	11.4
	EDZ-4	47.8	1.0	-	-	-	14.4	-	-	6.3
	EDZ-3	17.2	0.3	-	-	-	9.6	-	-	2.9
	EDZ-2	98.7	0.7	131	445	29.4	8.2	592	320	8.1
	EDZ-1	225	0.6	-	-	-	13.7	-	-	19.3
Frontal Zone	E3	72.1	2.4	238	687	34.6	12.9	529	257	7.7
Open ocean	S4	40.2	4.5	-	-	-	16.9	-	-	4.3
	S3	30.7	4.0	42.8	101	42.3	14.5	346	148	2.6
	E2	22.3	4.4	78.0	116	67.5	12.2	387	168	2.3
	S2	34.1	7.8	-	-	-	13.9	-	-	2.1
	S1	12.2	1.6	-	-	-	5.4	-	-	0.7
	E1	11.7	2.3	12.3	25.8	47.6	6.7	19.7	6.3	0.8

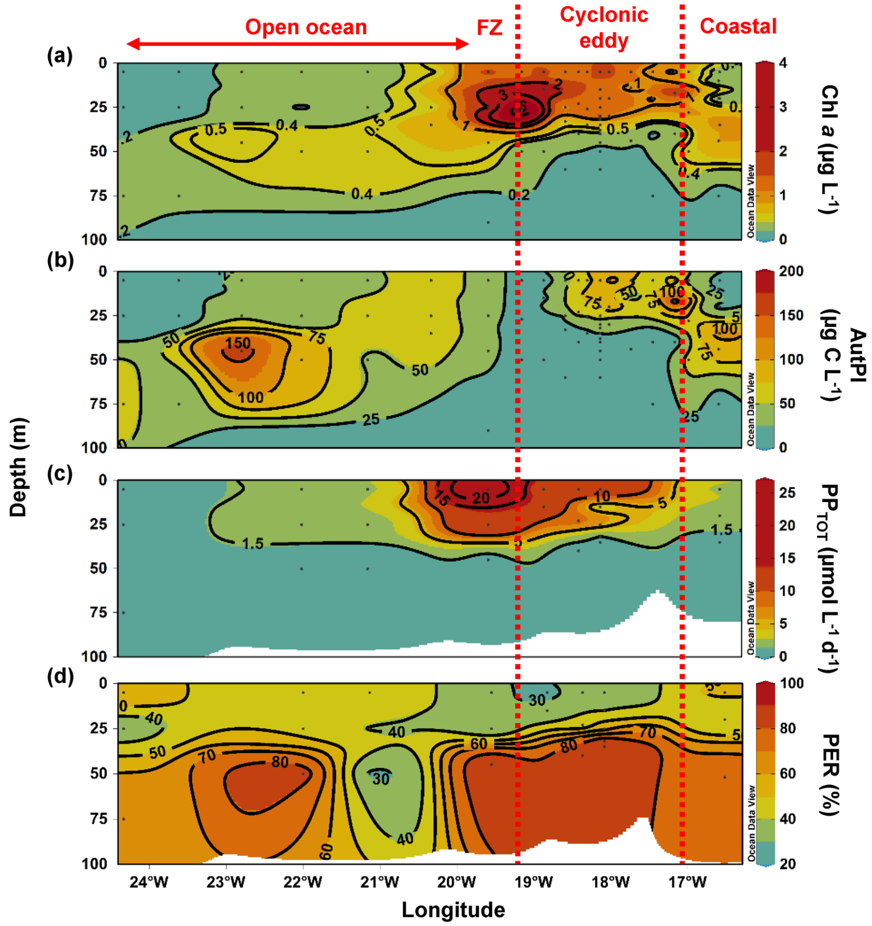

Figure 3: Depth distribution of phytoplankton biomass and activity over 100m depth: Chlorophyll *a* (Chl *a;* **a**), Autotrophic plankton biomass (AutPl; **b**), total primary production (PP_{TOT}; **c**), and percentage of extracellular release (PER; **d**). Red dashed line show the eddy-influenced area and FZ refer as Frontal Zone.

3.3 Bacterial abundance and activities

Heterotrophic bacterial abundance decreased with depth and was highest in the upper 50 m of all stations (Fig. **4a**). At the coastal and open ocean stations, integrated (0-100 m depth) heterotrophic bacteria abundance ranged between 12.9-14.7 and 5.4-16.9x10^{15} cells m^{-2}, respectively (Table **1**). No significant differences in heterotrophic bacterial abundance were observed between the open ocean and coastal stations (Tukey, *p*>0.05). In the open ocean waters, the lowest integrated BR and CR rates (Table 1) were reported at the station furthest offshore (24.33 °W), with 6.3 and 19.7 mmol C m^{-2} d^{-1}, respectively. Yet in the other open ocean stations (21.13 to 22 °W), integrated BR and CR rates were higher (148-168 and 346-348 mmol C m^{-2} d^{-1} respectively) than in the coastal station (32 and 98 mmol C m^{-2} d^{-1} respectively). Overall, BR and CR rates were higher in the open ocean than at the coastal stations with high rates (> 1 and > 2.5 µmol C L^{-1} d^{-1}, respectively) down to 60 m depth (Fig. **4b**; SI Fig. **S5a**). Integrated BP, in contrast, was generally higher at the coastal stations with 2.9-5.7 mmol C m^{-2} d^{-1} compared to the open ocean with 0.7-4.3 mmol C m^{-2} d^{-1} (Table **1**). However, BP rates were not significantly different from the open ocean (Tukey $p>0.05$), where BP rates were more variable. At the coastal stations, the highest BP (Fig. **4b**) rates were observed at the surface (5 m) and around ~40 m depth, while in the open ocean, the highest rates were found at the surface (5 m). BGE was determined for the upper 50 m (Table **2**) and showed only little variability over depth. However, BGE was significantly higher (Tukey, $p < 0.05$) at the coastal than at the open ocean stations with ranges of 5.3 ± 2.2 to 8.0 ± 1.0% compared to 0.9 ± 0.04 to 2.3 ± 0.02%, respectively. We estimated the predominance of autotrophy/heterotrophy in the system, by dividing the PP_{TOT} rates by the BCD. Heterotrophic conditions ($\frac{PP_{TOT}}{BCD}<1$) occurred at the open ocean stations throughout the water column, while autotrophic conditions ($\frac{PP_{TOT}}{BCD}>1$) prevailed at the coastal St. E5 (Table **2**). This pattern was preserved when data were integrated over the mixed layer (Fig. **5**) apart for the furthest station offshore (24.33 °W) where autotrophy occurred, yet lower than at the coastal station St.E5 ($\frac{PP_{TOT}}{BCD} = 2$ and 5.5 respectively). PP_{DOC} rates were sufficient to satisfy the BCD at the coastal St.E5 but not in the open ocean stations (Table **2**).

In the CE and at the Frontal Zone, integrated heterotrophic bacterial abundance ranged from 8.2 - 23.7x10^{15} cells m^{-2} (Table **1**). In the CE, substantial variation of bacterial abundance occurred within the upper 20 m (Fig. **4a**), with an abundance of <1x10^{9} cells L^{-1} in the western CE periphery (18.83 to 19.11 °W) and > 3x10^{9} cells L^{-1} in the CE core stations (~18 °W). Depth-integrated BR and CR (Table **1**) ranged between 59.1 and 320 and between 135 and 592 mmol C m^{-2} d^{-1}, respectively. Elevated BR and CR rates (> 1 and 2.5 µmol C L^{-1} d^{-1}, respectively) were only present in the upper ~30-40 m of the CE (Fig. **4b**; SI Fig. **S5a**). Integrated BP rates ranged from 2.9 to 19.3 mmol C m^{-2} d^{-1} in the CE and at the Frontal Zone stations (Table **1**). BP rates in the upper 40 m of the CE and at the Frontal Zone were elevated but were significantly higher than in the coastal and open ocean stations only in the stations within the CE periphery (Tukey $p<0.05$). Stations in the core of the CE had BGEs (Table **2**) significantly higher than the stations located in the open ocean (Tukey, $p<0.05$). BGE had a range of 1.4 ± 2.2 to 10.5 ± 0.5 % and 2.8 ± 0.1 to 3.0 ± 1.7% in the CE and the Frontal Zone stations, respectively. Highest BGE was observed below 20 m depth in the CE core (up to 10.48%, St EDM-4E). With ratios ranging from 1.13 to 3.5, the upper 40 m of the CE and the Frontal Zone stations were rather autotrophic (Table **2**). When integrated over the mixed layer (Fig. **5**), stations within the CE and at the Frontal Zone were autotrophic, with a $\frac{PP_{TOT}}{BCD}$ ratio ranging from 1.17 to 3.8. PP_{DOC} was on average 70% of the BCD within the CE and the Frontal Zone, yet ranging from 28.3 to 114.5%.

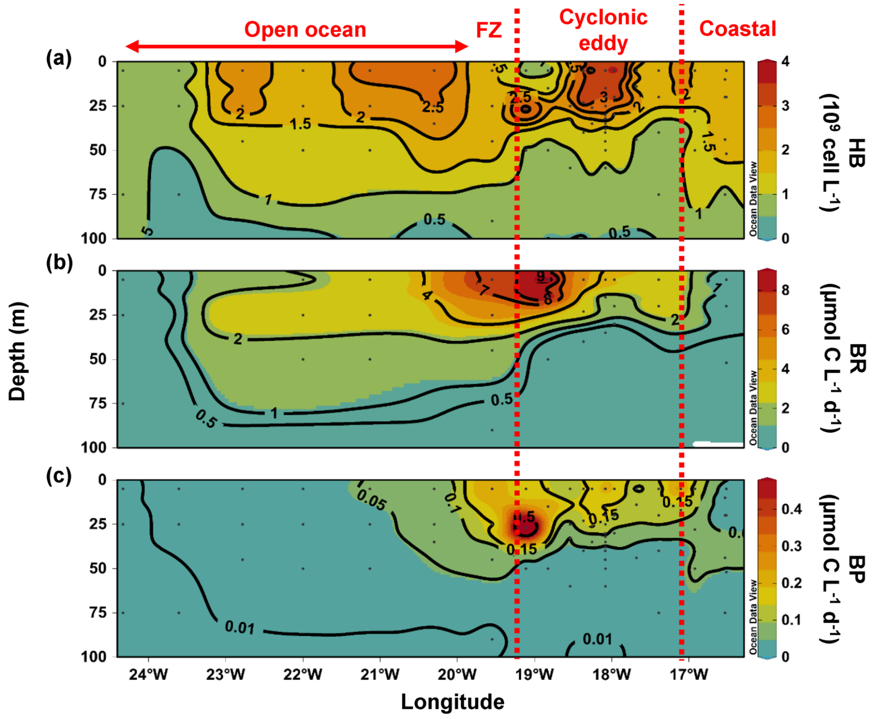

Figure 4: Depth distribution of bacterial abundance and microbial activities over 100m depth: Heterotrophic bacterial abundance (HB; **a**), bacterial respiration (BR; **b**), bacterial production (BP; **c**). Red dashed line show the eddy-influenced area and FZ refers to Frontal Zone.

Table 2: Average (mean) ± standard deviation of microbial metabolic activities during M156: bacterial carbon demand (BCD); bacterial growth efficiency (BGE); dissolved primary production (PP_{DOC}); Percentage of extracellular release (PER); total primary production (PP_{TOT}) and the ratio between BCD and PPTOT ($\frac{BCD}{PP_{TOT}}$). BCD and BGE were obtained from BP and BR rates at 22°C (see text). '-' indicate that the parameter was not measured and B.D. below detection (see text). PP_{DOC} and PP_{TOT} rates in St. EDM-4E were measured on the 22/07/2019 from 5, 33 and 50m depth and CR and BR rates were measured in St. E5 on the 29/07/2019 from 5, 35 and 50m depth.

Location	Station	Depth (m)	BCD (µmol C L^{-1} d^{-1})	BGE (%)	PP_{DOC} (µmol C L^{-1} d^{-1})	PER (%)	PP_{TOT} (µmol C L^{-1} d^{-1})	$\frac{BCD}{PP_{TOT}}$
Coastal	E5	5	0.6 ± 0.1	5.3 ± 2.2	1.5 ± 0.2	34.9 ± 1.1	2.7 ± 0.2	4.5 ± 1.5
		20	0.5 ± 0.1	6.9 ± 1.6	1.2 ± 0.1	52.6 ± 2.7	2.5 ± 0.1	5.5 ± 1.4
		35	0.5 ± 0.3	8.0 ± 1.0	0.7 ± 0.1	89.8 ± 3.9	1.0 ± 0.1	2.1 ± 0.2
	EDZ-10N	All	-	-	-	-	-	-
	S6	All	-	-	-	-	-	-
Eddy Periphery	EDZ-8N	All	-	-	-	-	-	-
	EDZ-7N	5	3.5 ± 0.7	3.6 ± 0.3	-	-	-	-
		20	3.5 ± 0.3	3.3 ± 1.7	-	-	-	-
	EDZ-6N	All	-	-	-	-	-	-
Eddy Core	EDZ-5N	5	2.6 ± 0.4	6.02 ± 1.5	-	-	-	-
		20	1.15 ± 0.3	9.51 ± 2.1	-	-	-	-
		30	0.41 ± 0.6	7.11 ± 0.2	-	-	-	-
		100	B.D.	B.D.	-	-	-	-
	EDM-4E	5	4.5 ± 0.4	4.1 ± 1.1	4.3 ± 0.1	36.7 ± 0.2	11.2 ± 0.1	2.5 ± 0.2
		15	1.3 ± 0.4	10.5 ± 0.6	0.4 ± 0.1	39.3 ± 6.8	1.1 ± 0.1	2.1 ± 0.4
		35	B.D.	B.D.	0.6 ± 0.3	94.4 ± 0.9	0.6 ± 0.3	-
		60	B.D.	B.D.	-	-	-	-
	EDM-3E	All	-	-	-	-	-	-
	EDM-4	5	4.7 ± 1.1	3.2 ± 1.4	4.3 ± 1.0	35.1 ± 5.7	12.6 ± 1.2	2.7 ± 1.1
		23	3.4 ± 0.2	4.4 ± 2.1	3.9 ± 0.2	35.7 ± 1.4	11.0 ± 0.3	3.2 ± 1.4
		40	B.D.	B.D.	0.3 ± 0.1	85.3 ± 7.1	0.3 ± 0.1	-
		100	B.D.	B.D.	-	-	-	-
Eddy Periphery	S5	5	-	-	4.8 ± 0.4	34.9 ± 1.1	13.7 ± 0.7	-
		25	-	-	3.4 ± 0.3	52.6 ± 2.7	6.5 ± 0.4	-
		32	-	-	0.2 ± 0.1	89.8 ± 3.9	0.2 ± 0.1	-

Table 2 cont.: Average (mean) ± standard deviation of microbial metabolic activities during M156: bacterial carbon demand (BCD); bacterial growth efficiency (BGE); dissolved primary production (PP_{DOC}); Percentage of extracellular release (PER); total primary production (PP_{TOT}) and the ratio between BCD and PPTOT ($\frac{BCD}{PP_{TOT}}$). BCD and BGE were obtained from BP and BR rates at 22°C (see text). '-' indicate that the parameter was not measured and B.D. below detection (see text).

Location	Station	Depth (m)	BCD (µmol C L^{-1} d^{-1})	BGE (%)	PP_{DOC} (µmol C L^{-1} d^{-1})	PER (%)	PP_{TOT} (µmol C L^{-1} d^{-1})	$\frac{BCD}{PP_{TOT}}$
Eddy Periphery	EDM-5E	All	-	-	-	-	-	-
	EDM-2E	All	-	-	-	-	-	-
	EDZ-4	All	-	-	-	-	-	-
	EDZ-3	All	-	-	-	-	-	-
	EDZ-2	5	10.5 ± 0.5	1.4 ± 2.2	2.9 ± 0.3	25.1 ± 3.4	11.9 ± 1.0	2.1
		15	9.4 ± 2.3	2.5 ± 0.7	4.9 ± 0.1	31.0 ± 1.7	14.5 ± 0.6	0.3
		50	B.D.	B.D.	-	-	-	-
		100	B.D.	B.D.	-	-	-	-
	EDZ-1	All	-	-	-	-	-	-
Frontal Zone	E3	5	7.1 ± 0.4	3.0 ± 1.7	7.8 ± 0.4	31.7 ± 1.7	25.0 ± 0.9	3.5 ± 2.2
		25	4.8 ± 1.1	2.8 ± 0.1	5.0 ± 0.6	33.4 ± 3.2	14.3 ± 0.8	3.0 ± 0.7
		45	1.9 ± 0.6	2.9 ± 2.1	0.7 ± 0.2	87.0 ± 3.3	0.8 ± 0.2	0.4 ± 0.3
		90	B.D.	B.D.	-	-	-	-
Open ocean	S4	All	-	-	-	-	-	-
	S3	5	3.2 ± 0.5	1.6 ± 0.2	1.3 ± 0.2	49.1 ± 5.5	2.7 ± 0.3	0.9 ± 0.5
		25	2.6 ± 0.5	1.7 ± 1.1	1.16 ± 0.03	38.4 ± 0.9	2.5 ± 0.03	1.0 ± 0.3
		50	1.2 ± 1.1	1.8 ± 0.2	0.0 ± 0.01	21.8 ± 6.6	0.1 ± 0.01	0.1 ± 0.1
		100	B.D.	B.D.	-	-	-	-
	E2	5	1.8 ± 0.6	1.8 ± 0.2	0.6 ± 0.1	40.9 ± 3.4	1.38 ± 0.1	0.8 ± 0.1
		25	3.5 ± 1.1	0.9 ± 0.04	0.94 ± 0.1	50.2 ± 3.1	1.89 ± 0.1	0.5 ± 0.1
		50	1.7 ± 0.4	1.6 ± 0.4	1.25 ± 0.3	91.3 ± 2.5	1.4 ± 0.3	0.8 ± 0.8
		100	B.D.	B.D.	-	-	-	-
	S2	All	-	-	-	-	-	-
	S1	All	-	-	-	-	-	-
	E1	5	0.4 ± 0.2	2.3 ± 0.02	0.23 ± 0.1	54.7 ± 13.3	0.39 ± 0.1	0.9 ± 0.5
		25	B.D.	B.D.	0.18 ± 0.01	38.5 ± 0.6	0.43 ± 0.01	-
		75	B.D.	B.D.	0.08 ± 0.02	61.7 ± 6.2	0.13 ± 0.02	-
		125	B.D.	B.D.	-	-	-	-

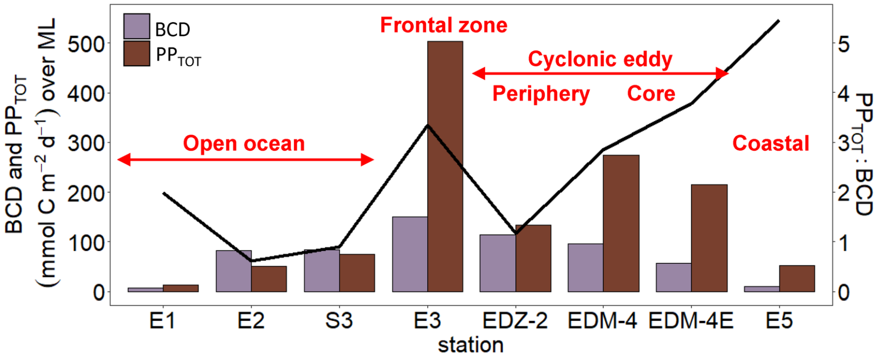

Figure 5: Integrated total primary production (PP$_{TOT}$) and bacterial carbon demand (BCD) rates over the mixed layer during M156. Blackline reports the ratio between PP$_{TOT}$ and BCD. More information are given in SI table 1.

3.4 Indices of phyto- and bacterioplankton activity change

We investigated the impact of the CE on heterotrophic bacterial and phytoplankton abundance by regression analysis of, cell-specific BR and BGE (Fig. **6a**), as well as autotrophic plankton biomass and Chl-*a* (Fig. **6b**). We noticed a negative semilogarithmic relationship (Fig. **6a**) between cell-specific BR rates and the BGE in both the zonal transect (coastal+open ocean) [BG= -3.11 ln (cell-specific BR) + 2.35; R^2=0.86; p<0.001] and the eddy influenced region (CE + Frontal Zone) [BGE= -1.92 ln (cell-specific BR) + 5.28; R^2=0.70; p=0.001]. Concerning the phytoplankton (Fig. **6b**), we observed that Chl-*a* and autotrophic plankton biomass were linearly correlated in the open ocean and coastal region (R^2=0.75; p<0.001) while being poorly correlated in the CE-influenced area (R^2=0.13).

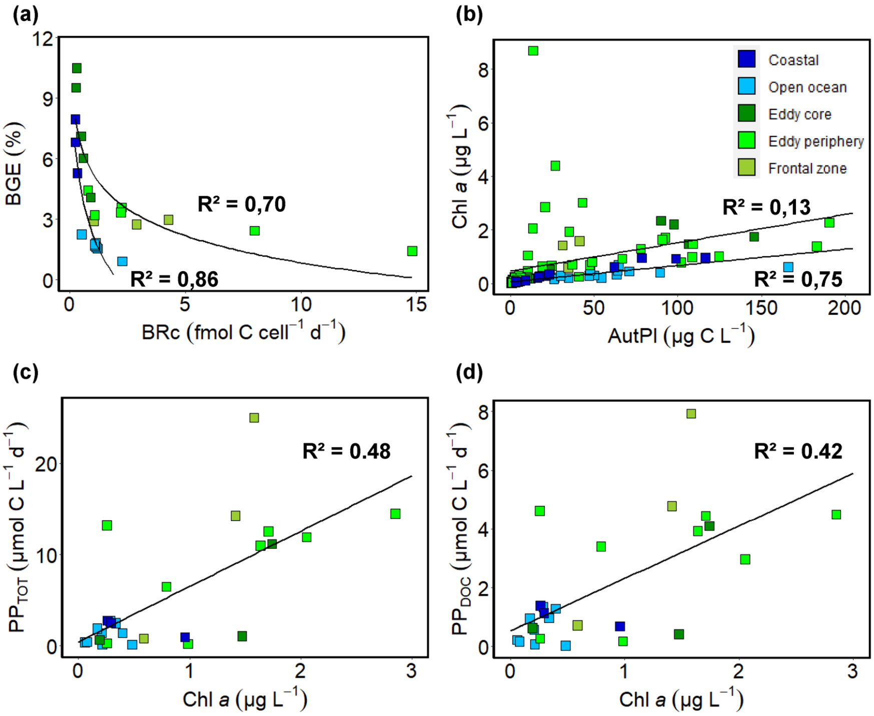

Figure 6: Relationship between (**a**) cell-specific bacterial respiration (BRc) and bacterial growth efficiency (BGE), (**b**) chlorophyll *a* (Chl *a*) and autotrophic plankton biomass (AutPl), (**c**) total primary production (PP$_{TOT}$) and Chl *a* and (**d**) dissolved primary production (PP$_{DOC}$) and Chl *a*. Black lines in (**a**) and (**b**) show regression from the open ocean and coastal stations (blue shades) and from the stations in eddy influenced area (green shades). Black lines in (**c**) and (**d**) show regressions in all the stations.

3.5 Semi-labile dissolved organic carbon

Between coastal and open ocean stations, SL-DOC concentration was not significantly different (Tukey, *p*>0.05; SI Fig. **S5b**) with ranges of 1.9-8.0 µmol L^{-1} and 4.7-18.9 µmol L^{-1}, respectively. At those sites, SL-DOC distribution was rather uniform in the upper 40 m with SL-DOC > 5 µmol L^{-1}, apart from the station furthest offshore from 22.7-24.3 °W where SL-DOC > 5 µmol L^{-1} was limited to shallow depth (5 m). In the CE and at the Frontal Zone, SL-DOC concentration was clearly elevated and increased from East to West with an overall range of 1.4-54.3 µmol L^{-1}. At the Frontal Zone, SL-DOC concentration > 5 µmol L^{-1} was detectable down to 90 m depth.

3.6 Correlation analysis

We applied a Pearson correlation matrix (Fig. **7**) to reveal significant correlations between the measured parameters. Temperature correlated negatively with nutrients (DIN, PO_4, $Si(OH)_4$; Pearson, $R<-0.9$, $p<0.001$) and positively with bacteria (Pearson, $R=0.65$, $p<0.001$). Total (PP_{TOT}) and dissolved primary production (PP_{DOC}) were positively correlated to each other (Pearson, $R=0.98$, $p<0.001$) and to Chl-*a* and SL-DOC (Pearson, $R>0.65$ and >0.60 respectively, $p<0.001$), but not to the autotrophic plankton biomass (Pearson, $R<0.14$, $p>0.05$). Bacterial biomass production (BP) and respiration (BR) were positively correlated (Pearson, $R=0.78$, $p<0.001$). BCD was more correlated to BR than to BP (Pearson, $R=1$ and $R=0.74$ respectively, $p<0.001$). A clear coupling between phytoplankton and bacteria was indicated, by positive correlations between PP_{TOT} and PP_{DOC} and BP, BR, and BCD (Pearson, $R>0.70$, $p<0.001$), BP and Chl-*a* (Pearson, $R=0.93$, $p<0.001$), and BR and Chl-*a* and the SL-DOC concentration (Pearson, $R=0.78$ and 0.75 respectively, $p<0.001$).

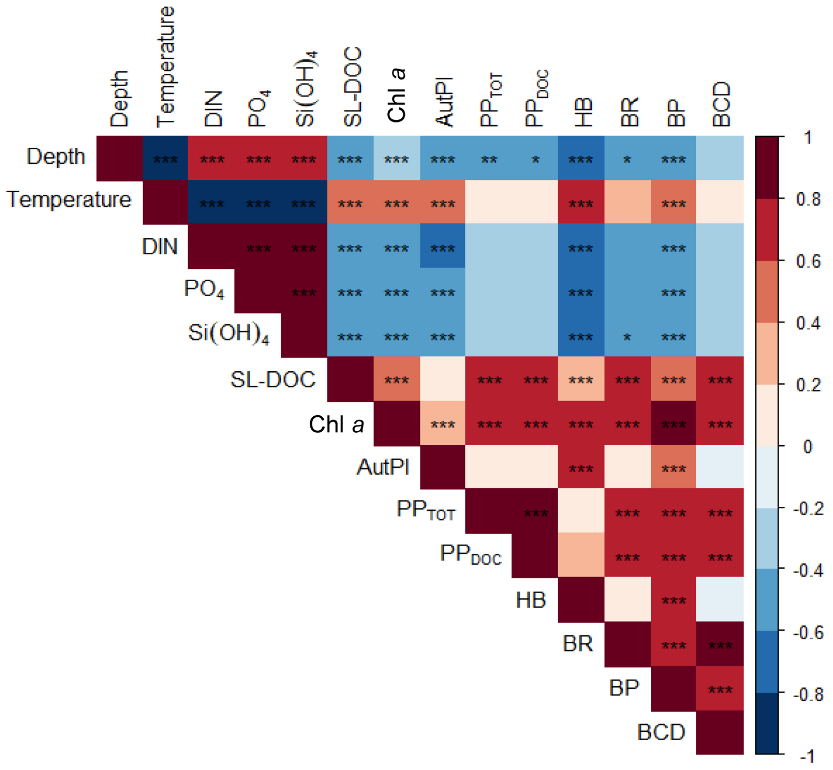

Figure 7: Correlations of biochemical parameters, metabolic activities, and bacterial abundance in the upper 200 m during M156. Colour scale: correlation coefficient (r). Statistical significance: '***'< 0.001, '**'< 0.01, '*'< 0.05.

4. Discussion

4.1 Distribution of phytoplankton abundance and activity in the Mauritanian upwelling system associated with cyclonic eddy perturbation

In general, coastal Chl-*a* concentration during this study was not as high as observed in earlier studies with strong coastal upwelling (e.g. Alonso-Sáez et al., 2007; Agustí and Duarte, 2013; Arístegui et al., 2020). This might be related to the relatively weak upwelling, as a result of weak surface winds along the Mauritanian Coast typically occurring during summer when our samples were collected (Peligrí and Peña-Izquierdo, 2015a). Consequently, during summer, fewer nutrients reach the euphotic zone by coastal upwelling, while offshore surface wind remains strong and might enhance vertical mixing at the surface. Coastal Chl-*a* concentration was only slightly higher compared to the open ocean, and both the coastal and open ocean phytoplankton communities were dominated by cells <20µm, as indicated by the strong linear correlation between Chl-a and autotrophic plankton biomass (Fig. 6b).

We did not observe a marked gradient in phytoplankton productivity either, unlike other regions of the CanUS with permanent upwelling conditions (Demarcq and Somoue, 2015; Arístegui et al., 2020). PP_{TOT} rates stayed rather constant from the coast to the open ocean and were in the range of reported rates in oligotrophic offshore waters of the CanUS (Agustí and Duarte, 2013; Lasternas et al., 2014). SL-DOC was relatively constant as well, with variations attributable to the westward propagation of the currents and eddies (SI Fig. **S5b**; Lovecchio et al., 2017, 2018). The absence of upwelling and the dominance of small autotrophic cells (<20µm) in the phytoplankton community suggest that in the open ocean and coastal stations, primary productivity was maintained through remineralisation of nutrients released from dying cells. Indeed, plankton mortality rates have been reported to increase with decreasing cell size (Marbá et al., 2007) and with increasing PER (Lasternas et al., 2014). Agustí and Duarte (2013) reported PER to range from ~1% in 'healthy' communities from the upwelled waters of the CanUS to ~70% in 'dying' communities from the oligotrophic waters of the ETNA. PER in our study was on average 51.1 ± 17% in the open ocean and coastal stations leading to the conclusion that primary productivity in those areas was maintained mainly through remineralisation of small (<20µm) plankton cells.

The CE broke this rather uniform distribution of phytoplankton productivity and community through coastal and open ocean waters. From a depth distribution perspective, Chl-*a* isolines seemed to have been pushed toward the surface in the CE (Fig. **3a**). Similar 'compression' of Chl-*a* isolines towards the surface have been reported in eddies earlier (Lochte and Pfannkuche 1987; Feng et al., 2007; Noyon et al., 2019). Such compressions have been attributed to resulting from phytoplankton growth through upwelling of nutrients combined with high vertical mixing from strong surface winds, which favour phytoplankton distribution at the surface (Feng et al., 2007; Noyon et al., 2019). In the CE, the upwelling was marked by the hydrographic parameters (e.g. temperature, salinity, nutrients, Fig. **2**), and before the eddy survey, strong surface winds occurred offshore (SI Fig. **S7**). Therefore, the phytoplankton which grew from upwelled nutrients must have been relocated to the surface through mixing,

https://doi.org/10.5194/bg-2022-49
Preprint. Discussion started: 21 February 2022

the reason why high Chl-*a* (>0.5 µg L^{-1}) concentration was found at the surface (5m) in all stations within the CE.

In addition, Chl-*a* was dispatched differently within the CE with the highest concentrations in the Western and Northern part and lowest concentrations in the Southern and Eastern part (Table **1**; SI Fig. **S4**). Furthermore, an almost continuous deepening of high Chl-a (>0.5 µg L^{-1}) distribution, as well as an increase of SL-DOC concentration, was observed in the CE from East to West (Fig. **3a**; SI Fig. **S5b**). Chelton et al. (2011) established from satellite observation and an eddy-centric perspective that due to the rotational flow and the westward propagation of CEs Chl-*a* tends to accumulate in their Southwest quadrants while being lower in their Northeast quadrants. Since in our case, the CE shape was elliptic, we assume that the rotational flow in the CE changed, shifting the accumulation. To the best of our knowledge, this is the first time that high-resolution sampling could demonstrate this specific submesoscale Chl-*a* distribution within a CE.

Outside of the CE boundaries, we noticed a thermal front with colder surface water. Thermal fronts are often detected out of eddies periphery as a consequence of eddy-eddy interaction (See review by Mahadevan, 2016) and/or eddy-wind interaction (Xu et al., 2019). In this Frontal Zone, we observed higher nutrient content than the adjacent stations and a doming of the nutriclines marking an upwelling (Fig. **2a**, **d-f**). Thus, Chl-*a* was elevated, and 'compressed' to the surface similarly as in the CE (Fig. **3a**). We assume this distribution to be the consequence of the same factors affecting the CE (upwelling, mixing induced by strong surface winds).

In the CE-influenced area (CE+Frontal Zone), Chl-*a* concentration was disconnected from small (<20µm) autotrophic plankton biomass (Fig. **6b**). This implies that in the West of the eddy where Chl-*a* was high and small autotrophic plankton biomass low (Fig. **3a & b**), larger autotrophic cells such as diatoms and/or dinoflagellate were present in higher quantities. We corroborate this point from lipid biomarkers concentration (unpublished data) as fucoxanthin, a typical marker of diatoms (Stauber and Jeffrey, 1998), was the dominant pigment in the Western part of the CE. This is consistent with previous studies in which CEs unevenly altered the phytoplankton community, often reporting the presence of diatoms/dinoflagellates (e.g., Lochte and Pfannkuche, 1987; Lasternas et al., 2013). The details of autotrophic plankton composition (SI Fig. **S7**) confirm this diversity, with the uneven distribution of cyanobacteria (Synechococcus) and eukaryotic pico- and nanoplankton within the CE underscoring the fact that the phytoplankton community was likely separate from the transect and diverse within a submesoscale range.

Therefore, the CE dispatched different phytoplankton taxa with different potentials of primary production and resources acquisition. Moreover, the mixed layer was also highly variable within the CE leading to substantial variation of PP_{TOT} rates (SI Table **1**, Figure **5**). Hence, we observed a three-fold variation of depth-integrated PP_{TOT} rates over 100m depth (Table **1**) within the CE which is coherent with earlier observations of a fivefold variation of primary production integrated over the euphotic zone in a CE in the subtropical Pacific Ocean (Falkowski et al., 1991). Overall, primary productivity was enhanced within the CE and the Frontal Zone with an average of fourfold more depth-integrated PP_{TOT} rates over 100m depth than in the open ocean and coastal stations. This is coherent with Löscher et al. (2015) who found that depth-integrated primary productivity over the chlorophyll *a* maximum of a CE in the Mauritanian upwelling system was threefold higher than the surrounding waters. Exudation rates (PP_{DOC}) were also enhanced within the eddy and integrated (0-100 m) PP_{DOC} rates were on average three-fold time higher than in the transect (Table **1**). Yet, even if PP_{DOC} rates were higher within the CE and at the Frontal Zone stations (Table **2**), PER was slightly lower at the surface (Fig. **3d**). We start from two hypotheses regarding this distribution 1) the lower PER reported was due to a higher proportion of larger phytoplankton (e.g. diatoms) who have lower turnover rates and therefore have lower PER and/or 2) the upwelling of nutrients generated by the CE might have enhanced the physiological health of the phytoplankton community (Agustí and Duarte, 2013; Laternas and Agustí, 2014).

4.2 Heterotrophic bacteria abundance and activities responses in the Mauritanian upwelling system

Along the zonal transect (open ocean+coastal stations), a strong coupling between HB abundance and PP_{TOT} rates was observed ($R^2=0.72$). Therefore, HB abundance followed the same trends as the PP_{TOT} by being continuously distributed from the coast to the offshore waters. Bachmann et al. (2018) reported a similar trend in the Mauritanian upwelling system during summer, strengthening our finding.

Bacterial activities were distributed differently. Both BR and BP were within the range of reported rates for coastal and offshore water of the CanUS (Reinthaler et al., 2006; Alonso-Saez et al., 2007; Vaqué et al., 2014).BP rates slightly decreased from the coast to the open ocean. Similar trends were found in the CanUS with different upwelling intensities and at different seasons (Alonso-Saez et al., 2007; Vaqué et al., 2014). Therefore, those factors (upwelling intensity and seasonality) were likely only indirectly coupled with BP variability, which instead was rather driven by the composition of the phytoplankton community. Indeed, BP was more correlated to Chl-*a* than autotrophic plankton biomass (<20µm; Fig. **7**) suggesting that BP was more enhanced by the presence of larger autotrophic cells, such as diatoms or dinoflagellates. Those have larger phycospheres allowing them to attract more bacteria by chemotaxis (see review by Seymour et al., 2017). Hence, bacteria may benefit from mutualistic relationships with larger algae increasing their BP. Fucoxanthin, was decreasing from the coastal to offshore waters with overall low relative abundance (5-15%) (data not shown). Being part of microphytoplankton, especially diatoms have higher viability in coastal than in offshore waters of the CanUS (Lasternas et al., 2013), which may explain the observed fucoxanthin gradient.

In contrast, BR rates were higher in offshore than in coastal waters. BR rates were coupled to SL-DOC concentration, which is in agreement with Xu et al. (2013), who also found BR to be enhanced by low molecular weight DOC compound (<30kDa). SL-DOC compounds have a turnover of weeks to months, which allows them to escape rapid microbial degradation (Hansell et al., 2009). In the CanUS, currents and eddies can laterally transport DOC up to 2000 km (Lovecchio et al., 2018). Hence, we state that SL-DOC compounds produced at the coast have been relocated offshore while being slowly respired by heterotrophic bacteria along the way.

The distinct distribution of BP and BR rates affected the distribution of the BGE, which was higher in the coastal than in the open ocean stations. This is in accordance with observations by Alonso-Sáez et al. (2007) who showed higher BGE in the upwelling area above Cape Blanc than in the offshore waters of the CanUS. Overall, the BGEs reported here are among the lowest reported with all values <11%, but not surprising since BGE is negatively correlated to temperature and, therefore, reduced in the tropical ocean (Rivkin and Legendre, 2001). Yet we report an average BGE three times lower than Alonso-Sáez et al., (2007). We assume this difference to result from the difference in upwelling intensity (none vs. permanent). Indeed, Kim et al. (2017) denoted that BGE increased with increasing upwelling intensity in the Ulleung Basin. Under none or low upwelling conditions, bacteria compete with phytoplankton for nutrient acquisition. Moreover, as microphytoplankton do not thrive in the water column due to their high nutrient requirements (see review by Marañón, 2015), bacteria benefit less from their phycospheres. Hence, we expect BP to be lower in the relaxation period (May to July) post upwelling than in the upwelling season (January to March; Lathuilière et al., 2008) in the Mauritanian upwelling system.

Within the CE-influenced stations (CE + Frontal Zone), HB abundance was disconnected from the PP_{TOT} rates (Fig. **4a**). HB abundance was significantly higher in the core of eddy but surprisingly low at the Southwestern side of the eddy periphery (18.83 to 19.11 °W), where both PP_{TOT} rates and Chl-*a* were high (Fig. **3a**, **c**). Hernández-Hernández et al. (2020) reported a similar feature with a strong disparity of HB biomass distribution within a CE in the CanUS. Since Chl-*a* and SL-DOC compounds accumulated in the Southwestern part of the CE, gel-likes particles produced by phytoplankton and bacteria such as transparent exopolymer particles (TEP) (Passow, 2002) might have also accumulated there. We hypothesize that a missing fraction of the bacteria might have been attached to gel-like particles (Busch et al., 2018) or other particulate matter.

The BP was particularly stimulated within the CE-influenced stations and on average threefold higher than in the open ocean stations when integrated over 100 m. This is in accordance with earlier studies from the Sargasso Sea (Ewart et al., 2008), the CanUS (Baltar et al., 2010), and in the Mediterranean Sea (Belkin et al., 2022) where CEs enhanced BP. As stated previously, the upwelling induced by the CE and the Frontal Zone led to higher phytoplankton biomass, including diatoms and/or dinoflagellates which were likely responsible for this increase in BP.

BR rates were also enhanced at the surface of the CE and were coupled to the SL-DOC concentration. Since the CE was relatively young (1.5 months old), autochthonous SL-DOC compounds produced by exudation (PP_{DOC}) must have been merged with allochthonous coastal SL-DOC compounds transported during the CE formation. PP_{DOC} rates in the CE covered 28.3 to 114.5% of the BCD, indicating a moderate to strong trophic dependence of bacteria on phytoplankton in CE (Fouilland and Mostajir, 2010). Although PP_{TOT} may satisfy the BCD in the CE through the bacterial incorporation of phytoplankton-derived DOC from sloppy feeding, exudation, viral infection, or cell apoptosis, a question remains about why heterotrophs preferentially used SL-DOC compounds for respiration rather than for biomass production. We start from two hypotheses, firstly, the SL-DOM compounds had a high C/N ratio leading to an increase of BR and a decrease of BGE (Lønborg et al., 2011). Secondly, SL-DOC was easier to access for bacteria than other nutrients. Phytoplankton-DOM exudate/lysates are more or less labile following their origin (e.g. diatoms/cyanobacteria) and are depleted in the nutrient (e.g. nitrate/phosphate) limiting phytoplankton growth (e.g. Pete et al., 2010; Wear et al., 2020). As the phytoplankton community was diverse within the CE and as the CE likely transported allochthonous DOM, a multitude of compounds with specific qualities coexisted in the CE. Therefore, bacteria may have used SL-DOC as fuel to degrade DOM compounds containing limiting nutrients for their growth (Guillemette et al., 2016).

The diversity of DOM from different origins (e.g. cyanobacteria/diatom) within the CE likely induced distinct bacterial communities. We noticed a negative semilogarithmic relationship (Fig **6**) between cell-specific BR and the BGE in both the zonal transect (coastal+open ocean stations) and the CE influenced (CE + Frontal Zone) stations. The slopes of the curves and the ranges of cell-specific BR values were different between the two systems suggesting distinct bacterial communities with different degrees of resource optimization (Baña et al., 2014). Within the CE, the bacterial community was probably as the phytoplankton community even more diverse as observed in previous CEs studies (Zhang et al., 2011; Yan et al., 2018).

Our results show that bacteria do not grow proportionally to the amount of DOM they received through exudation but rather depends on the different requirement between respiration and biomass production. In response, the BGE varied sevenfold within the CE (1.4-10.5%) whereas it varied twofold in the open ocean (0.9-2.3%) and in the coastal (5.3-7.9%) stations. Robinson (2008) suggested that most of the BGE variability within oligotrophic waters is explained by BR. Here we hypothesise that in CEs, which cross oligotrophic waters in the ETNA, BGE variability depends on both BP through phytoplankton taxonomical composition and BR through the amount and quality of the SL-DOC.

Overall, we showed that autotrophy prevails in the upper 100m depth of Mauritanian coastal waters while heterotrophy prevailed offshore. This is coherent with a modeling study from Lovecchio et al. (2017). The CE and the associated Frontal Zone fuelled phytoplankton nutrients needs and maintained autotrophy offshore. The highest PP_{TOT} and the most pronounced autotrophy were determined at the Frontal Zone. Mouriño-Carballido (2009) reported from indirect estimations of net community production that the frontal zones between CEs and ACEs are among the most productive area in the North West subtropical Atlantic Ocean. Previous studies showed that the trophic balance could switch from autotrophy to heterotrophy in an eddy within a month(s) (Maixandeau et al., 2003; Mouriño-Carballido et al., 2006). Here we report with a small timescale (11 days) that in a CE, states of little to high autotrophy occurred. Thus, phytoplankton dynamic and associated bacterial responses within eddies not only change with time but also through space. This urges the need for more high-resolution eddy studies in order to better estimate their impact on plankton metabolic activities and carbon cycling.

Conclusion

Our results highlight the ability of a CE to be an autotrophic vector towards the open ocean with organic matter freshly produced by the phytoplankton community inside. Yet, despite the strong autotrophy associated with the CE, phytoplankton exudation of DOM was not always enough to compensate for bacterial metabolic needs. Even if BP was enhanced in the CE, the BGE was low and varied substantially. This implies that heterotrophic bacteria recycle allochtonous DOM transported by the eddy and/or have issues to degrade phytoplankton DOM. Microbial metabolic activities dynamic within eddies are complex and require further investigations to understand and unravel the carbon cycling.

Data availability

All data will be made available at the PANGEA database (data manager, webmaster: Hela Mehrtens)

Author contribution

QD, KWB and AE designed the scientific study, analyzed the data and wrote the paper. AB, did the eddy reconstruction and both AE and JH commented on the paper.

Competing interests:

The authors declare that they have no conflict of interest.

Acknowledgments

We thank the captain and the crew of the *R/V Meteor* for their support during the M156 cruise. We thank J. Roa, T. Klüver and L. Scheidemann for sampling on board. We thank J. Roa and S. Golde additionally for the analysis of dissolved organic matter and T. Klüver for cell counting, bacterial and phytoplankton activities analyses. We thank B. Domeyer and R.

Suhrberg for the nutrient analyses. This study has been conducted using E.U. Copernicus Marine Service Information. The results contain modified Copernicus Climate Change Service information 2020. Neither the European Commission nor ECMWF is responsible for any use that may be made of the Copernicus information or data it contains. This study is a contribution of the REEBUS project (Role of Eddies in the Carbon Pump of Eastern Boundary Upwelling Systems) sub-projects WP1 and WP4, funded by the BMBF (funding reference no. 03F0815A).

Reference

Agustí, S., and Duarte, C. M.: Phytoplankton lysis predicts dissolved organic carbon release in marine plankton communities, Biogeosciences, 10, 1259-1264, https://doi.org/10.5194/bg-10-1259-2013, 2013.

Alonso-Sáez, L., Gasol, J. M., Arístegui, J., Vilas, J. C., Vaqué, D., Duarte, C. M., and Agustí, S.: Large-scale variability in surface bacterial carbon demand and growth efficiency in the subtropical northeast Atlantic Ocean, Limnol. Oceanogr., 52, 533-546, https://doi.org/10.4319/lo.2007.52.2.0533, 2007.

Anderson, T. R., and Ducklow, H. W.: Microbial loop carbon cycling in ocean environments studied using a simple steady-state model, Aquat. Microb. Ecol., 26, 37-49. 2001.

Arístegui, J., Barton, E. D., Álvarez-Salgado, X. A., Santos, A. M. P., Figueiras, F. G., Kifani, S., Hernández-León, S., Mason, E., Machú, E., and Demarcq, H.: Sub-regional ecosystem variability in the Canary Current upwelling, Prog. Oceanogr., 83, 33-48, https://doi.org/10.1016/j.pocean.2009.07.031, 2009.

Arístegui, J., Montero, M. F., Hernández-Hernández, N., Alonso-González, I. J., Baltar, F., Calleja, M. L., and Duarte, C. M.: Variability in Water-Column Respiration and Its Dependence on Organic Carbon Sources in the Canary Current Upwelling Region, Front. Earth Sci., 8, 1-12. https://doi.org/10.3389/feart.2020.00349/, 2020.

Arístegui, J., Tett, P., Hernández-Guerra, A., Basterretxea, G., Mon- tero, M. F., Wild, K., Sangrá, P., Hernández-León, S., Cantón, M., García-Braun, J. A., Pacheco, M., and Barton, E. D.: The influence of island-generated eddies on Chl a distribution: a study of mesoscale variation around Gran Canaria, Deep-Sea Res., 44:71-96. 1997.

Baltar, F., Arístegui, J., Gasol, J. M., Lekunberri, I., & Herndl, G. J.: Mesoscale eddies: Hotspots of prokaryotic activity and differential community structure in the ocean. ISME J., 4, 975-988, https://doi.org/10.1038/ismej.2010.33, 2010.

Baña, Z., Abad, N., Uranga, A., Azúa, I., Artolozaga, I., Unanue, M., Iriberri, J., Arrieta, J. M., and Ayo, B.: Recurrent seasonal changes in bacterial growth efficiency, metabolism and community composition in coastal waters. Environ. Microbiol., 22, 369-380, https://doi.org/10.1111/1462-2920.14853. 2020.

Baña, Z., Ayo, B., Marrasé, C., Gasol, J. M., and Iriberri, J.: Changes in bacterial metabolism as a response to dissolved organic matter modification during protozoan grazing in coastal Cantabrian and Mediterranean waters, Environ. Microbiol., 16, 498-511, https://doi.org/10.1111/1462-2920.12274, 2014.

Bergkvist, J., Klawonn, I., Whitehouse, M. J., Lavik, G., Brüchert, V., & Ploug, H.: Turbulence simultaneously stimulates small- and large-scale CO2 sequestration by chain-forming diatoms in the sea. Nat. Commun., 9, 1-10, https://doi.org/10.1038/s41467-018-05149-w, 2018.

Bergstedt, M. S., Hondzo, M. M., and Cotner, J. B.: Effects of small scale fluid motion on bacterial growth and respiration, Freshw. Biol., 49, 28-40, https://doi.org/10.1046/j.1365-2426.2003.01162.x, 2004.

Briand, E., Pringault, O., Jacquet, S., and Torréton, J. P.: The use of oxygen microprobes to measure bacterial respiration for determining bacterioplankton growth efficiency. Limnol. Oceanogr. Meth., 2, 406-416, https://doi.org/10.4319/lom.2004.2.406, 2004.

Busch, K., Endres, S., Iversen, M. H., Michels, J., Nöthig, E. M., and Engel, A.: Bacterial colonization and vertical distribution of marine gel particles (TEP and CSP) in the arctic Fram Strait, Front. Mar. Sci., 4, 1-9. https://doi.org/10.3389/fmars.2017.00166, 2017.

Carr, M. E.: Estimation of potential productivity in Eastern Boundary Currents using remote sensing, Deep-Sea Res. II: Top. Stud. Oceanogr., 49, 59-80, https://doi.org/10.1016/S0967-0645(01)00094-7, 2001.

Cheney, R. E., and Richardson, P. L.: Observed Decay of a Cyclonic Gulf Stream Ring, Deep-Sea Res. Oceanogr. Abstr., 23, 143-155, https://doi.org/10.1016/S0011-7471(76)80023-X, 1976.

https://doi.org/10.5194/bg-2022-49
Preprint. Discussion started: 21 February 2022

Couespel, D., Lévy, M., & Bopp, L.: Oceanic primary production decline halved in eddy-resolving simulations of global warming, Biogeosciences, 18(14), 4321-4349, https://doi.org/10.5194/bg-18-4321-2021, 2021.

D'Asaro, E. A.: Generation of submesoscale vortices: A new mechanism, J. Geophys. Res., 93, 6685-6693, https://doi.org/10.1029/JC093iC06p06685, 1988.

del Giorgio, P. A., and Cole, J. J.: Bacterial Growth Efficiency in Natural Aquatic Systems. Annu. Rev. Ecol. Evol. Syst., 29, 503-541, https://doi.org/10.1146/annurev.ecolsys.29.1.503, 1998.

Demarcq, H. and Somoue, L.: Phytoplankton and primary productivity off Northwest Africa. In: Oceanographic and biological features in the Canary Current Large Marine Ecosystem. Valdés, L. and Déniz-González, I. (eds). IOC-UNESCO, Paris. IOC Technical Series, No. 115, pp. 161-174. URI: http://hdl.handle.net/1834/9186.2015.

Descy, J. P., Leporcq, B., Viroux, L., François, C., & Servais, P.: Phytoplankton production, exudation and bacterial reassimilation in the River Meuse (Belgium). J. Plankton Res., 24(3), 161-166. https://doi.org/10.1093/plankt/24.3.161, 2002.

Dickson, A. G., Sabine, C. L., and Christian, J. R.: Guide to Best Practices for Ocean CO2 measurements. PICES Special Publication 3, 191 pp., 2007.

Dittmar, T., Cherrier, J., and Ludwichowski, K. U.: The analysis of amino acids in seawater, in: Practical guidelines for the analysis of seawater, ed. by Oliver Wurl Boca Raton [u.a.], CRC Press, ISBN: 978-1-4200-7306-5, 2009.

Dray, S.: On the number of principal components: A test of dimensionality based on measurements of similarity between matrices, Comput. Stat. Data Anal., 52, 4, 2228-2237, 2008.

Eichinger, M., Sempéré, R., Grégori, G., Charrière, B., Poggiale, J. C., and Lefèvre, D.: Increased bacterial growth efficiency with environmental variability: Results from DOC degradation by bacteria in pure culture experiments, Biogeosciences., 7(6), 1861-1876, https://doi.org/10.5194/bg-7-1861-2010, 2010.

Engel, A., and Galgani, L.: The organic sea-surface microlayer in the upwelling region off the Coast of Peru and potential implications for air-sea exchange processes. Biogeosciences, 13(4), 989-1007, https://doi.org/10.5194/bg-13-989-2016, 2016.

Engel, A., Goldthwait, S., Passow, U., and Alldredge, A.: Temporal decoupling of carbon and nitrogen dynamics in a mesocosm diatom bloom. Limnol. Oceanogr. 47, 753-761, doi: 10.4319/lo.2002.47.3.0753, 2002.

Engel, A., Händel, N., Wohlers, J., Lunau, M., Grossart, H. P., Sommer, U., and Riebesell, U.: Effects of sea surface warming on the production and composition of dissolved organic matter during phytoplankton blooms: Results from a mesocosm study, J. Plankton Res., 33(3), 357-372, https://doi.org/10.1093/plankt/fbq122, 2011.

Evans, C. A., O'Reily, J. E., and Thomas, J. P.: A handbook for measurement of Chl a a and primary production, College Station, TX: Texas A &M University, 1987.

Ewart, C. S., Meyers, M. K., Wallner, E. R., McGillicuddy, D. J., and Carlson, C. A.: Microbial dynamics in cyclonic and anticyclonic mode-water eddies in the northwestern Sargasso Sea, Deep-Sea Res. II: Top. Stud. Oceanogr., 55(10-13), 1334-1347. https://doi.org/10.1016/j.dsr2.2008.02.013, 2008.

Falkowski, P. G., Ziemann, D., Kolber, Z., and Bienfang P. K.: Role of eddy pumping in enhancing primary production in the ocean, Letters to Nature, Vol 352, 1991.

Feng, M., Majewski, L. J., Fandry, C. B., and Waite, A. M.: Characteristics of two counter-rotating eddies in the Leeuwin Current system off the Western Australian coast, Deep-Sea Res. II: Top. Stud. Oceanogr., 54(8-10), 961-980, https://doi.org/10.1016/j.dsr2.2006.11.022, 2007.

Fischer, T., Karstensen, J., Dengler, M., and Bendinger, A.: Multiplatform observation of cyclonic eddies during the REEBUS experiment, EGU General Assembly 2021, online, 19-30 Apr 2021, EGU21-6537, https://doi.org/10.5194/egusphere-egu21-6537, 2021.

Gargas, E.: A Manual for Phytoplankton Primary Production Studies in the Baltic, The Baltic Marine Biologists, 2, 88 p., 1975.

Gattuso J. P., Epitalon J. M., Lavigne H. and Orr J.,: seacarb: seawater carbonate chemistry, R package version 3.2.13, http://CRAN.R-project.org/package=seacarb, 2020.

Gruber, N., Lachkar, Z., Frenzel, H., Marchesiello, P., Münnich, M., McWilliams, J. C., Nagai, T., and Plattner, G. K.: Eddy-induced reduction of biological production in eastern boundary upwelling systems. Nat. Geosci., 4(11), 787-792, https://doi.org/10.1038/ngeo1273, 2011.

Guillemette, F., Leigh McCallister, S. and del Giorgio, P.: Selective consumption and metabolic allocation of terrestrial and algal carbon determine allochthony in lake bacteria, ISME J., 10, 1373-1382, https://doi.org/10.1038/ismej.2015.215, 2016.

Hansell, D. A., Carlson, C. A., Repeta, D. J., & Schlitzer, R.: Dissolved organic matter in the ocean a controversy stimulates new insights. Oceanogr., 22(SPL.ISS. 4), 202–211. https://doi.org/10.5670/oceanog.2009.109, 2009.

Hernández-Hernández, N., Arístegui, J., Montero, M. F., Velasco-Senovilla, E., Baltar, F., Marrero-Díaz, Á., Martínez-Marrero, A., and Rodríguez-Santana, Á.: Drivers of Plankton Distribution Across Mesoscale Eddies at Submesoscale Range, Front. Mar. Sci., 7, 1-13. https://doi.org/10.3389/fmars.2020.00667, 2020.

Ihaka R., and Gentleman R.: R: a language for data analysis and graphics. J. Comput. Graph. Stat. 5, 299, 1996

Karstensen, J., Fiedler, B., Schütte, F., Brandt, P., Körtzinger, A., Fischer, G., Zantopp, R., Hahn, J., Visbeck, M., and Wallace, D.: Open ocean dead zones in the tropical North Atlantic Ocean, Biogeosciences, 12, 2597-2605, https://doi.org/10.5194/bg-12-2597-2015, 2015.

Kim, B., Kim, S. H., Kwak, J. H., Kang, C. K., Lee, S. H., & Hyun, J. H.: Heterotrophic bacterial production, respiration, and growth efficiency associated with upwelling intensity in the Ulleung Basin, East Sea. Deep Sea Res. Part II Top. Stud. Oceanogr., 143, 24-35, https://doi.org/10.1016/j.dsr2.2017.07.002, 2017.

Kirchman, D., K'nees, E., and Hodson, R.: Leucine incorporation and its potential as a measure of protein synthesis by bacteria in natural aquatic systems, Appl. Environ. Microbiol., 49(3), 599-607, https://doi.org/10.1128/aem.49.3.599-607.1985, 1985.

Lasternas, S., and Agustí, S.: The percentage of living bacterial cells related to organic carbon release from senescent oceanic phytoplankton, Biogeosciences, 11, 6377-6387, https://doi.org/10.5194/bg-11-6377-2014, 2014.

Lasternas, S., Piedeleu, M., Sangrà, P., Duarte, C. M., and Agustí, S.: Forcing of dissolved organic carbon release by phytoplankton by anticyclonic mesoscale eddies in the subtropical NE Atlantic Ocean. Biogeosciences, 10(3), 2129-2143, https://doi.org/10.5194/bg-10-2129-2013, 2013.

Lathuilière, C., Echevin, V., and Lévy, M.: Seasonal and intraseasonal surface Chl a-a variability along the northwest African Coast, J. Geophys. Res. Oceans, 113, C05007. https://doi.org/10.1029/2007JC004433, 2008.

Le Vu, B., Stegner, A., Arsouze, T.: Angular momentum eddy detection and tracking algorithm (AMEDA) and its application to coastal eddy formation, J. Atmos. Oceanic Technol. 35, 739-762. https://doi.org/10.1175/JTECH-D-17-0010.1, 2018.

Lee, M. M., and Williams, R. G.: The role of eddies in the isopycnic transfer of nutrients and their impact on biological production, J. Mar. Res., 58(6), 895-917, https://doi.org/10.1357/002224000763485746, 2000.

Lévy, M., Klein, P., and Treguier, A. M.: Impact of submesoscale physics on production and subduction of phytoplankton in an oligotrophic regime, J. Mar. Res., 59(4), 535-565, 2001.

Lindroth P., Mopper K.: High performance liquid chromatographic determination of subpicomole amounts of amino acids by precolumn fluorescence derivatization with o-phthaldialdehyde, Anal. Chem., 51, 1667-1674, https://doi:10.1021/ac50047a019, 1979.

Lochte, K., and Pfannkuche, O.: Cyclonic cold-core eddy in the eastern North Atlantic. II. Nutrients, phytoplankton and bacterioplankton, Mar. Ecol. Prog. Ser., 39, 153-164. https://doi.org/10.3354/meps039153, 1987.

López-Urrutia, Á., and Morán, X. A. G.: Resource limitation of bacterial production distorts the temperature dependence of oceanic carbon cycling, Ecology, 88(4), 817-822, https://doi.org/10.1890/06-1641, 2007.

Löscher, C. R., Fischer, M. A., Neulinger, S. C., Fiedler, B., Philippi, M., Schütte, F., Singh, A., Hauss, H., Karstensen, J., Körtzinger, A., Künzel, S., and Schmitz, R. A.: Hidden biosphere in an oxygen-deficient Atlantic open-ocean eddy: Future implications of ocean deoxygenation on primary production in the eastern tropical North Atlantic, Biogeosciences, 12, 7467-7482, https://doi.org/10.5194/bg-12-7467-2015, 2015.

Lovecchio, E., Gruber, N., & Münnich, M: Mesoscale contribution to the long-range offshore transport of organic carbon from the Canary Upwelling System to the open North Atlantic. Biogeosciences, 15(16), 5061–5091. https://doi.org/10.5194/bg-15-5061-2018, 2018.

Lovecchio, E., Gruber, N., Münnich, M., and Lachkar, Z.: On the long-range offshore transport of organic carbon from the Canary Upwelling System to the open North Atlantic, Biogeosciences, 14(13), https://doi.org/10.5194/bg-14-3337-2017, 2017.

Mahadevan, A.: The Impact of Submesoscale Physics on Primary Productivity of Plankton, Annu. Rev. Mar. Sci., 8, 161-184, https://doi.org/10.1146/annurev-marine-010814-015912, 2016.

Maixandeau, A., Lefevre, D., Karayanni, H., Christaki, U., VanWambeke, F., Thyssen, M., Denis, M., Fernandez, C.I., Uitz, J., Leblanc, K., Queguiner, B.: Microbial community production, respiration, and structure of the microbial food web of an ecosystem in the northeastern Atlantic Ocean, J. Geophys. Res. Oceans, 110 (C7), C07S17, 2005.

Marañón E, Cermeño P, Fernández E, Rodríguez J, Zabala L.: Significance and mechanisms of photosynthetic production of dissolved organic carbon in a coastal eutrophic ecosystem, Limnol Oceanogr, 49, 1652−1666, 2004.

Marbá, N., Duarte, C. M., and Agustí, S.: Allometric scaling of plant mortality rate, P. Natl. Acad. Sci. USA, 104, 15777–15780, 2007.

McGillicuddy Jr, D. J., Anderson, L. A., Doney S. C., and Maltrud, M. E.: Eddy-driven sources and sinks of nutrients in the upper ocean : Results from a 0 . 1 ° resolution model of the North Atlantic, Glob. Biogeochem. Cycles., 17(2), 1035, https://doi.org/10.1029/2002GB001987, 2003.

McGillicuddy, D. J., and Robinson, A. R.: Eddy-induced nutrient supply and new production in the Sargasso Sea, Deep-Sea Res. I: Oceanogr. Res. Pap., 44(8), 1427-1450, https://doi.org/10.1016/S0967-0637(97)00024-1, 1997.

McGillicuddy, D. J.: Mechanisms of Physical-Biological-Biogeochemical Interaction at the Oceanic Mesoscale, In Annual Review of Marine Science (Vol. 8), https://doi.org/10.1146/annurev-marine-010814-015606, 2016.

Mied, R. P., J. C. McWilliams, and Lindemann G. J.: The generation and evolution ofmushroom-like vortices, J. Phys. Oceanogr., 21,489-510, 1991.

Molemaker, M. J., McWilliams, J. C., and Dewar, W. K.: Submesoscale generation of mesoscale anticyclones near a separation of the California Undercurrent, J. Phys. Oceanogr., 45, 613-629, https://doi.org/10.1175/JPO-D-13-0225.1, 2015.

Mouriño-Carballido, B., and McGillicuddy, D. J.: Mesoscale variability in the metabolic balance of the Sargasso Sea, Limnol. Oceanogr., 51(6), 2675-2689, https://doi.org/10.4319/lo.2006.51.6.2675, 2006.

Mouriño-Carballido, B.: Eddy-driven pulses of respiration in the Sargasso Sea, Deep-Sea Res. I: Oceanogr. Res. Pap., 56(8), 1242-1250, https://doi.org/10.1016/j.dsr.2009.03.001, 2009.

Neijssel, O. M., and Mattos, M. J. T. De.: Micro Review The energetics of bacterial growth : a reassessment, 13(2), 179-182, 1994.

Nielsen, E. S.: The use of radio-active carbon (c14) for measuring organic production in the sea, ICES Mar. Sci., 18(2), 117-140, https://doi.org/10.1093/icesjms/18.2.117, 1952.

Noyon, M., Morris, T., Walker, D., & Huggett, J.: Plankton distribution within a young cyclonic eddy off south-western Madagascar, Deep Sea Res. Part II Top. Stud. Oceanogr., 166, 141-150, https://doi.org/10.1016/j.dsr2.2018.11.001, 2018.

Passow, U.: Transparent exopolymer particles (TEP) in aquatic environments, Prog. Oceanogr., 55(3-4), 287-333, https://doi.org/10.1016/S0079-6611(02)00138-6, 2002.

Pete, R., Davidson, K., Hart, M. C., Gutierrez, T., and Miller, A. E. J.: Diatom derived dissolved organic matter as a driver of bacterial productivity: The role of nutrient limitation, J. Exp. Mar. Biol. Ecol., 391(1-2), 20-26, https://doi.org/10.1016/j.jembe.2010.06.002, 2010.

Rao, D. N., Chopra, M., Rajula, G. R., Durgadevi, D. S. L., and Sarma, V. V. S. S.: Release of significant fraction of primary production as dissolved organic carbon in the Bay of Bengal, Deep Sea Res. Part I Oceanogr. Res., 168, 1-27, https://doi.org/10.1016/j.dsr.2020.103445, 2021.

Regaudie-De-Gioux, A., and Duarte, C. M.: Temperature dependence of planktonic metabolism in the ocean. Glob. Biogeochem. Cycles, 26(1), GB1015, https://doi.org/10.1029/2010GB003907, 2012.

Reinthaler, T., Bakker, K., Manuels, R., van Ooijen, J., & Herndl, G. J.: Erratum to Fully automated spectrophotometric approach to determine oxygen concentrations in seawater via continuous-flow analysis. Limnol. Oceanogr. Methods 5(1), 72–72. https://doi.org/10.4319/lom.2007.5.72, 2007.

Robinson C.: Heterotrophic bacterial respiration. In: Kirchman DL (ed) Microbial ecology of the oceans, Wiley-Liss, New York, NY., 2008.

Russell, J. B. and Cook, M. G.: Energetics of Bacterial Growth : Balance of Anabolic and Catabolic Reactions, Microbiol Rev., 59(1), 48-62, 1995.

Schartau, M., Engel, A., Schröter, J., Thoms, S., Völker, C., and Wolf-Gladrow, D.: Modelling carbon overconsumption and the formation of extracellular particulate organic carbon, Biogeosciences, 4, 433-454, 2007.

Schlitzer, R.: Ocean Data View, odv.awi.de, 2020.

Schütte, F., Brandt, P., and Karstensen, J.: Occurrence and characteristics of mesoscale eddies in the tropical northeastern Atlantic Ocean, Ocean Sci., 12, 663-685, https://doi.org/10.5194/os-12-663-2016, 2016.

Seymour, J. R., Amin, S. A., Raina, J. B., and Stocker, R.: Zooming in on the phycosphere: The ecological interface for phytoplankton-bacteria relationships. Nat. Microbiol., 2, 17065, https://doi.org/10.1038/nmicrobiol.2017.65, 2017.

Simon, M., and Azam, F.: Protein content and protein synthesis rates of planktonic marine bacteria, Mar. Ecol. Prog. Ser., 51, 201-213, 1989.

Singh, A., Gandhi, N., Ramesh, R., & Prakash, S.: Role of cyclonic eddy in enhancing primary and new production in the Bay of Bengal, J. Sea Res, 97, 5-13, https://doi.org/10.1016/j.seares.2014.12.002, 2015.

Smith, D., and Azam, F.: A simple, economical method for measuring bacterial protein synthesis rates in seawater using. Mar. Microb. Food Webs, 6(2), 107-114, 1992.

Solorzano, L.: Determination of Ammonia in Natural Waters by the Phenolhypochlorite Method, Limnol. Oceanogr., 14, 799-801, 1969.

Strickland, J.D.H. and Parsons, T.R.: A Practical Handbook of Seawater Analysis. Bulletin of Fisheries Research Board of Canada, 167, 1-311, 1968.

Thomsen, S.: The formation of a subsurface anticyclonic eddy in the Peru-Chile Undercurrent and its impact on the near-coastal salinity, oxygen, and nutrient distributions, J. Geophys. Res. Oceans, 121, 476-501, https://doi.org/ 10.1002/2015JC010878, 2016.

Thornton, D. C. O.: Dissolved organic matter (DOM) release by phytoplankton in the contemporary and future ocean, Eur. J. Phycol., 49(1), 20-46, https://doi.org/10.1080/09670262.2013.875596, 2014.

Vaqué, D., Alonso-Sáez, L., Arístegui, J., Agustí, S., Duarte, C. M., Montserrat Sala, M., Vázquez-Domínguez, E., and Gasol, J. M.: Bacterial production and losses to predators along an Open ocean productivity gradient in the Subtropical North East Atlantic Ocean. J. Plankton Res., 36(1), 198-213, https://doi.org/10.1093/plankt/fbt085, 2014.

Wear, E. K., Carlson, C. A., and Church, M. J.: Bacterioplankton metabolism of phytoplankton lysates across a cyclone-anticyclone eddy dipole impacts the cycling of semi-labile organic matter in the photic zone, Limnol. Oceanogr., 65(7), 1608-1622, https://doi.org/10.1002/lno.11409, 2020.

Wickham H.: tidyverse: Easily Install and Load 'Tidyverse' Packages. See https://cran. r-project.org/package=tidyverse, 2016.

Wilhelm, W. L.: Die Bestimmung des im Wasser gelösten Sauer- stoffes, Ber. Dtsch. Chem. Ges., 21, 2843-2854, 1888.

Wood, A. M., and van Valen, L. M.: Paradox lost? On the release of energy-rich compounds by phytoplankton, Mar. Microb. Food Webs, 4, 103-116, 1990.

Xu, G., Dong, C., Liu, Y., Gaube, P., and Yang, J.: Chl a Rings around Ocean Eddies in the North Pacific, Sci. Rep., 9(1), 1-8, https://doi.org/10.1038/s41598-018-38457-8, 2019.

Xu, J., Jing, H., Sun, M., Harrison, P. J., and Liu, H.: Regulation of bacterial metabolic activity by dissolved organic carbon and viruses, J. Geophys. Res. Biogeosci., 118(4), 1573-1583, https://doi.org/10.1002/2013JG002296, 2013.

Yan, W., Zhang, R., and Jiao, N.: A longstanding complex tropical dipole shapes marine microbial biogeography, Appl. Environ. Microbiol., 84(18), https://doi.org/10.1128/AEM.00614-18, 2018.

Zhang, Y., Jiao, N., Sun, Z., Hu, A., & Zheng, Q.: Phylogenetic diversity of bacterial communities in South China Sea mesoscale cyclonic eddy perturbations, Res. Microbiol., 162(3), 320–329, https://doi.org/10.1016/j.resmic.2010.12.006, 2011.